Tribology performance, airborne particle emissions and brake squeal noise of copper-free friction materials

L. Wei, Y.S. Choy*, C.S. Cheung, D. Jin

Department of Mechanical Engineering, The Hong Kong Polytechnic University, Hung Hom, Kowloon, Hong Kong

*Corresponding author.
Tel: +852 2766 7813
Email: mmyschoy@polyu.edu.hk

Abstract

Copper and its alloy have been widely used in the formulation of non-asbestos organic (NAO) friction materials as reinforcements and/or additives. But U.S.A has raised a legislation to reduce the copper content in friction materials due to the toxicity of copper in wear debris. Thus, there is a need to develop copper-free friction materials which also owns the desired tribology performance. In the present study, two new copper-free non-asbestos organic (NAO) friction materials were developed by replacing the copper fiber with steel fiber (named SFM) or ceramic fiber (named CFM). Friction and wear behaviors, airborne wear particle emissions and brake squeal noise of these two copper-free friction materials were evaluated and compared with a reference copper containing friction material (RFM) by using a pin-on-disc test rig. Results show that all friction materials have comparable friction coefficients, and the specific wear rates of SFM and CFM are larger than that of RFM. The mean fractal dimension of RFM surface is larger than those of SFM and CFM surfaces. For the airborne particle emissions, RFM presents the lowest particle number emissions and particle mass concentrations (PMCs) of PM_{10} (particles smaller than 10 μm) and SFM presents the highest values of these two results. For brake squeal noise, the brake squeal noise of all friction materials has comparable A-weighted sound pressure levels (SPLs). It can be concluded that the

replacement of copper fiber with steel and ceramic fibers can obtain comparable tribology performance and brake squeal noise, but it will increase the particle emissions.

Key words: Disc brakes; Copper-free friction materials; Airborne wear particle emissions; Brake squeal noise

Nomenclature

BSE	backscatter electron
CFM	ceramic fiber friction material
COF	coefficient of friction
CPC	condensation particle counter
DMA	differential mobility analyzer
EDXS	energy-dispersive X-ray spectroscopy
GMD	geometric mean diameter
HEPA	high efficiency particle absorber
LM	low metallic
NAO	non-asbestos organic
PM	particulate matter
PMC	particle mass concentration
RFM	reference friction material
SEM	scanning electron microscopy
SFM	steel fiber friction material
SI	supplementary information
SM	semi metallic
SMPS	scanning mobility particle sizer
SPL	sound pressure level
TEOM	tapered element oscillating microbalance
TNC	total number concentration

1. Introduction

Brake pad materials for motor vehicles contain a lot of ingredients that can be classified into four categories: reinforcing fibers, binders, fillers and friction additives [1, 2]. Copper is one of the commonly used reinforcing fibers and/or friction additives [2, 3]. The primary reason for the use of copper is to increase the thermal conductivity and eliminate thermal fade of brake pads [4]. In addition, some studies reported that copper fibers could help to achieve a smooth sliding condition and reduce the possibility for noise generation [3, 5]. Österle et al. [3] reported that the copper nano-particles, produced from the severe plastic deformation of copper fibers, could work as solid lubricant similar to graphite particles which accommodated the velocity between rotating disc and fixed pad and reduced the fluctuation of friction force. This phenomenon is mainly due to the equiaxed structure of copper nanoparticles which were incorporated into the friction layer easily. Ho et al. [5] investigated the tribological and mechanical characteristics of semi-metallic (SM) friction materials using copper, brass, steel, cellulose, carbon and ceramic fibers as the reinforcing fiber respectively. They found that the copper fiber provided relatively high and stable coefficient of friction (COF) and low wear among all fibers. Barros et al. [6] found that the increment of copper content in SM friction materials could decrease the COF and reduce the disc wear. Kumar and Bijwe et al. [7] investigated the role of copper on the tribology performance and the morphology of worn surface of non-asbestos organic (NAO) friction materials with various amounts and shapes of copper. They reported copper powders performed better in improving the wear resistance than copper fibers and there were no cracks and ingredient degradation on the brake pad surface for the friction materials containing copper powders.

However, in 2015, the Environmental Protection Agency of United States and the automotive industry signed a memorandum of understanding to reduce the copper content in brake pads to less than 5% by weight in 2021 and 0.5% by weight in 2025 because copper in brake wear debris is one main source for copper in highway stormwater runoff and can be discharged into the waterways near the road [8]. Copper can cause the rapid death of aquatic organisms due to its neurobehavioral toxicity [9-11]. Several studies have been conducted on the possibility of replacing the copper fiber with some other fibers in recent years. Leonardi et al. [12] replaced the copper fiber in a low-metallic (LM)

friction material with steel fiber and reported that partial replacement of copper fiber with steel fiber kept the COF at the similar value while increased the specific wear rate. Menapace et al. [13] replaced the copper fibe in a NAO friction material with barite and found that the use of barite improved the wear resistant of brake pad and also obtained a stable variation of COF against time. Mahale et al. [14] replaced the copper fiber in NAO friction material with stainless steel swarf and found that the copper fiber brake pad exhibited better performance in recovery ratio and wear, while steel swarf brake pad had better friction performance during the fade and recovery cycle. Jang et al. [15] found the copper fiber containing friction material and steel fiber containing friction material had the similar COF under different sliding velocities and contact pressures but the steel fiber containing friction material had higher specific wear rate. Kumar et al. [16] investigated the roles of copper, brass and steel fibers in the friction and wear behaviours of NAO friction materials and found the copper and brass fibers based friction materials exhibited better friction and wear performance than steel fiber based friction material.

During braking process, some wear debris become air borne particles that will be emitted into the environment. Brake wear particles account for 16-55% by mass of non-exhaust PM_{10} emissions and 11-21% by mass of total traffic-related PM_{10} emissions at urban environments of Europe [17]. Moreover, since regulations for exhaust particle emissions become more and more strict and there are no regulations for non-exhaust particle emissions, relative contribution of non-exhaust particle emissions to the total traffic-related particle emissions will continually increase. Nosko et al. [18] compared the airborne wear particle emissions from different friction materials by using a pin-on-disc test-rig and found airborne wear particle emissions from copper containing friction material were comparable to other friction materials. Lyu et al. [19] compared the friction, wear and airborne wear particle emissions between two copper-free brake pads and one copper-containing brake pad and reported that the copper-free brake pads produced more airborne particle emissions than the copper-containing brake pad. In the literature, some studies explored the possibility of replacing copper fibers with some other fibers or powders, but few of them considered the influence of substitutions on airborne wear particle emissions.

Braking noise is another important issue that should be considered when exploring substitutions of copper fibers in friction materials. Up to 60% of brake system related warranty issues are related to brake noise [20]. Brake squeal is a type of brake noise with the main frequencies higher than 1 kHz that is generated from friction induced high frequency oscillation [21]. Its sound pressure level (SPL) commonly exceeds 70 dB or is 20 dB higher than the ambient noise level [22]. The brake squeal noise is a strongly nonlinear dynamic behaviour which is triggered by some external forces [21]. One of the major external sources is the local oscillation on the contact surface including the impacts and ruptures between contact plateaus [23] and the role of wear debris [24]. Chan et al. [25] found that local oscillation with large amplitude could be attributed to the severe exfoliation of friction layers on the brake pad surface and the formation of adhesively joined asperities. Eriksson et al. [26] explored the connection between contact surface topography and brake squeal occurrence. They found that the brake pad with many small contact plateaus generated more brake squeal noise than the brake pad with few large contact plateaus. Lee and Jang [27] reported that the contact plateaus distribution affected the oscillation amplitude and frequency of friction force. But they observed that the brake pad surface with a few large contact plateaus produced larger oscillation amplitudes than that with a lot of small contact plateaus. The conflicting results indicate that the effect of brake pad surface morphology on the friction induced vibration and brake squeal noise should be further analysed. From the previous studies, different surface morphologies reflect different local dynamic behaviors on the contact surface which cause different brake squeal noise. As introduced in our previous study [28], the brake pad surface morphology is closely related to the friction material formulation especially the metal content. Several studies have investigated the effects of metal content in friction materials on the brake squeal noise. Lazzari et al. [21] compared the propensities of different friction materials to generate brake squeal and found that the copper containing LM friction material had higher possibility to trigger brake squeal than NAO friction material. Kchaou et al. [22] investigated the influence of steel fibers in friction materials on the squeal noise and found that its main frequencies were in the range of 7 to 10 kHz, and cracks and material braking-off were observed on the brake pad surface after squealing events. But in the literature, few studies investigated the relationship between local

oscillation on the contact surface and brake squeal noise with different reinforcing fibers in friction materials. Moreover, brake squeal noise should be evaluated when developing new copper-free friction materials.

The purpose of the present study is to investigate the possibility of replacing the copper in NAO friction material with steel fiber or ceramic fiber taking into consideration of the airborne wear particle emissions and brake squeal noise. Regarding the airborne wear particle emissions, both particle number and particle mass concentrations are evaluated. Regarding the brake squeal noise, this study investigates the relationship between the local dynamic behaviour and brake squeal noise. The increase of steel fiber content in friction materials can improve their mechanical strength [16] and increase the friction coefficient and specific wear rate [15, 29]. As mentioned before, several studies compared the friction and wear behaviours between steel fiber containing friction materials and copper fiber containing friction materials and reported that the steel fiber have the potential to replace the copper fiber in friction materials. But there is still lack of study on evaluating the variations of airborne wear particle emission and brake squeal noise when replacing the copper fiber in NAO friction materials with steel fiber. Ceramic fibers can improve the mechanical strength of friction materials and friction and wear stabilization [30]. Due to the high thermal resistance, high mechanical strength and light weight of ceramic fiber, it should be possible to replace the copper fiber in friction materials. Since friction material formulation contains many ingredients, it is difficult to compare the friction and wear behaviours between ceramic fiber or steel fiber containing friction materials and copper fiber containing friction material from different studies. Thus, there is a need to compare the effects of ceramic, steel and copper fibers on the friction and wear behaviours, airborne wear particle emissions and brake squeal noise with the same friction material formulation. The present study developed two copper-free friction materials by replacing the copper fiber in the NAO friction material with steel or ceramic fibers. Experiments were conducted with a pin-on-disc test-rig. Friction and wear behaviours, characteristics of worn surfaces, airborne wear particle emissions and brake squeal noise were investigated to evaluate the performances of the copper, steel and ceramic fibers.

2. Experimental set-up

2.1. Preparation of friction materials

A typical formulation of copper containing NAO friction material was used to fabricate the reference friction material named as RFM which contains 10 ingredients [15]. The copper fiber content is 10% by volume. There are two types of copper-free friction materials: steel fiber friction material (SFM) and ceramic fiber friction material (CFM). SFM and CFM were fabricated by keeping 9 ingredients (identified as parent composition) constant and replacing the copper fiber with steel or ceramic fibers. The parent composition (90 vol%) contains 20 vol% of fibers (aramid pulp and steel fiber), 20 vol% of binder (phenolic resin), 20 vol% of friction additives (graphite, MoS_2, $ZrSiO_4$ and cashew dust) and 30 vol% of fillers ($BaSO_4$ and $Ca(OH)_2$). The specifications of fibers and friction material compositions are listed in Tables 1 and 2.

Friction materials were prepared following a typical manufacturing process for NAO friction material [4, 15, 31]. Firstly, all the raw materials were mixed up together using a shaker-mixer for 20 minutes. After mixing all the materials homogeneously, the mixture was placed into a cylindrical mold for a hot-pressing process. The hot-pressing pressure and duration were 15 MPa and 10 min respectively with a curing temperature of 150 ℃. After that, the mixture was post-cured at a temperature of 180 ℃ for 4 hr. Finally, the pin samples were cut from the mixture and machined to a cubic shape. They have a length of 10±0.2 mm and a height of 7±1 mm. The densities were calculated from the mass and geometric volume of mixtures as shown in Table 2. The surface hardness of pin samples was in the range of 40-46 HRM 100 independent from the friction material. Backscatter electron (BSE) images of prepared pin samples are show in Fig. 1. The discs were made of pearlitic grey cast iron with a diameter of 239 mm and a thickness of 9 mm. The surface hardness of grey iron discs was in the range of 90-93 HRB 100. The contact surfaces of pin samples and discs were not machined and kept as they were. Before each test, pin samples and discs were cleaned with dry air and ethanol respectively.

2.2. Test set-up and characterization techniques

2.2.1. Instruments for friction and wear performance

Braking tests were performed with a pin-on-disc tribometer as shown in Fig. 2. It is a reliable equipment to investigate the tribology performance of friction materials sliding against an iron disc and has been used in many previous studies [28, 32-34]. The detailed description of this tribometer is shown in our previous study [28]. An HBM ZLFC3/20 kg load cell was used to measure the tangential force with 1 Hz data recording rate. Hence, the friction coefficient can be calculated from the tangential force divided by the applied normal force. The pin sample temperature was measured with a K-type thermocouple and recorded every 10 seconds. It was placed inside the pin body at a distance of 2 mm from the contact surface. The specific wear rates (k_s) of the pin sample and disc were calculated using the following equation [12]:

$$k_s = \frac{\Delta V}{F_N \cdot \Delta s} \quad (1)$$

Where k_s is the specific wear rate in m^2/N; ΔV is the wear volume of the pin sample or disc in m^3; F_N is the applied normal force in N; Δs is the sliding distance in m. The wear volume of a pin sample was calculated from the mass loss and density in Table 2. The mass loss of pin sample was calculated by weighting the pin before and after each test using a VIBRA analytical balance with an accuracy of 0.01 mg. The wear volume of a disc was calculated from the transverse surface profile of wear track on the disc sample. The disc sample was cut from the disc using linear cutting. The surface profile was measured 3 times for each disc sample by using a Bruker DektakXT surface profiler. The brake discs after test mode 3 were selected to analyze the specific wear rate and surface morphology. Fig. S1 of supplementary information (SI) shows an example of the transverse surface profile of wear track used to calculate the wear volume of a disc. The friction layers on pin and disc surfaces were observed with a scanning electron microscope (SEM, JEOL Model JSM-6490) equipped with an energy dispersive X-ray spectroscopy (EDXS) detector.

The surface roughness of a brake pad surface is another important parameter which is related to the wear behaviour and the propensity to trigger brake squeal noise. However, the roughness parameters, such as slope and curvature, are influenced by the

resolution of the measuring instrument and sample length. To solve this problem, fractal dimension, a scale-invariant parameter, is used to describe the contact surface roughness because of its self-affinity (a small part can be considered as a reduced-scale image of the whole) [35-37]. Fractal dimension is calculated from the equation below [37]:

$$N(A > a) \quad a^{-(D_s - 1)/2} \tag{2}$$

Where N (A>a) is the total number of friction layers with areas larger than a particular value, a; D_s is the fractal dimension of a surface which can be obtained from the nonlinear curve fitting. In this study, the area of the smallest contact plateau that can be identified was about 800 μm^2. Thus, the smallest value of a is 800 μm^2. White points or areas smaller than 800 μm^2 were considered as noise and neglected in counting. Image-Pro Plus 6.0 was used to process the SEM images to calculate the fractal dimension of a pin sample surface. The picture processing procedure for fractal dimension is described in our previous study [28].

2.2.2. Instruments for airborne wear particle emissions

This pin-on-disc tribometer can also be used to investigate the airborne wear particles emitted from the disc brakes if it is placed in a sealed chamber as shown in Fig. 2. Its advantage is that the cleanness of ambient air in the chamber can be controlled so that all measured particles were generated from the wear process between the friction materials and disc. Similar equipment has been used to study the airborne wear particle emissions of disc brakes in some previous studies [38-41]. The compressed air flowed into the chamber through a high efficiency particle absorber, an air flow meter and an inlet opening connected by flexible tubes. The diameter of inlet opening was 30 mm. All connections to the chamber were sealed to prevent leakages, while the leakage had little impact on the experimental results because the air pressure inside the chamber was higher than outside [41]. In the chamber, the air was well mixed due to the complicated shape of the tribometer, the rotating of brake disc and the high air change rate [42, 43]. The air in the chamber transported the brake wear particles to outlet opening (diameter: 50 mm) for particle measurement.

The inlet air velocity was set to 0.28 m/s corresponding to an air flow rate of 47.5 liter/min. The volumes of chamber and pin-on-disc test-rig were 62 and 32 liters

247 respectively so that the air change ratio was about 94/hr. The high efficiency particle
248 absorber (HEPA) (Whatman Polycap 36 TF) was used to remove particles in the inlet air.
249 It has a retention efficiency of 99.97% for all particles larger than 0.3 μm. The
250 background particle concentrations in the sealed chamber ranged from 2.4-3.2 #/cm^3 in
251 most cases and reached 6 #/cm^3 in several tests. The background particles were measured
252 before and after each test by using a scanning mobility particle sizer (SMPS). As shown
253 in Fig. S2 of SI, they were only detected in several size classes which were much fewer
254 than those in particle emission results, in which particles were detected in the rage of 65-
255 104 size classes. The background particles accounted for 1.4-2% of the total particle
256 number concentrations. They were removed from the relevant particle number size
257 distribution and total number concentration results and had little impact on these two
258 results. The ambient air temperature was about 26 ℃ with the humidity of 58-62%. They
259 were not actively controlled, but almost constant during the experiments.
260 Airborne particles were transported to the outlet opening where the particles were
261 introduced to particle analyzers. Two instruments were used in this study. The first one
262 was the SMPS (model 3494) which consisted of a differential mobility analyzer (DMA
263 model 3071A), classifying the particle size according to their electric mobility, and a
264 condensation particle counter (CPC model 3022), determining the particle number
265 concentrations. The SMPS gave results of total number concentration (TNC), particle
266 number size distribution and geometric mean diameter (GMD). SMPS measured particles
267 in the size range of 15-750 nm and in 109 size classes. The SMPS was operated at a
268 sampling flow rate of 0.3 Liter/min with a sheath air flow of 3 Liter/min and gave a result
269 every 5 minutes. The second one was the tapered element oscillating microbalance
270 (TEOM, Series 1105). It measured the particle mass concentration (PMC) of particles
271 smaller than 10 μm (PM_{10}) in the range of 0.1 to 15000 μg/m^3 with 1 Hz data recording
272 rate. Its operation depends on the change of Eigen-frequency of the lever-filter unit due to
273 the deposition of particles on an oscillating filter. The sampling flow rate for the TEOM
274 ranged from 1 to 2.5 Liter/min. All results from the particle instruments are shown as
275 measured concentrations. The air flow rate through chamber was kept constant during
276 tests. Each test was conducted with a new pin sample. After each test, the surface of
277 tribometer and the inner surface of chamber were cleaned with ethanol.

2.2.3. Instruments for brake squeal noise

The pin-on-disc tribometer was also used to analyze the brake squeal noise as shown in Fig. 3. The present study focuses on the relationship between local dynamic behavior on the contact surface and brake squeal noise with different reinforcing fibers in the friction material. Therefore, a simplified test-rig is better than a full brake system because the system dynamic and boundary conditions can be controlled more easily. For a simplified test-rig, the differences of vibration and noise measurements between different friction materials are mainly caused by the relevant variation of local oscillation on the contact surface. Brake squeal phenomenon is very sensitive to the system dynamic and boundary conditions so that it is difficult to obtain repeatable squeal event from the complex real brake system [44]. But it is possible to produce some repeatable brake squeal noise by using a simplified test-rig. Another advantage is that the contact area in the simplified test-rig is much smaller than that in the real brake system which leads to a weak coupling between disc and pad holder. It allows to investigate the variation of brake parameters on the local dynamic behavior because the variation of system dynamic with the brake parameter is minor.

Two accelerometers were mounted on the brake pad holder to measure the vibration response in tangential and normal directions. A half inch microphone was placed 500 mm away from the center of rotating disc to record the sound signal. The location of microphone follows the suggestion in ref. [45]. Acceleration and sound signals were acquired with a B&K LAN-XI data acquisition hardware and processed with a commercial data processing software PULSE LabShop Version 20.0. The analyzed frequency range was 1k to 15k Hz with a frequency resolution of 25 Hz. The brake noise at frequencies below 1k Hz was not considered because it was generated from the vibration of mounting components of the pin sample which was different from the motor vehicle suspension system [46].

2.3. Design of experiments

The experiments were conducted at the sliding velocity of 2.8 m/s and at the applied forces of 52, 81 and 122 N, corresponding to the contact pressures (p) of 0.52, 0.81 and 1.22 MPa respectively. The $p \cdot v$ values range from 1.46-3.42 MPa·m/s which are typical light braking sequences of passenger vehicles under urban driving conditions [47].

The experimental duration was 90 minutes corresponding to a sliding distance of 15120 m. Pin temperature and friction coefficient were continuously recorded in each experiment. For SEM observation, there were four randomly selected SEM fields of view and eight measurements for each pin and disc samples to obtain reliable and repeatable results. For airborne particle emissions, particle number size distribution, TNC and GMD obtained from SMPS were measured five times in each test. PMC measured by TEOM was recorded for 10 minutes. For brake squeal noise, both acceleration and sound signals were recorded for 30 seconds in each measurement and they were measured five times in each test. Particle emissions and sound and acceleration signals were recorded when the friction force reached steady-state stage. Before the experiment, the background noise was recorded as shown Fig. S3 of SI. The A-weighted sound pressure level (SPL) of background noise was 40 dB. Experiments were repeated three times and the average results are shown in the present study. The average standard errors of the experimental results following the method in Moffat et al. [48], are shown in Table 3.

3. Results

3.1. Friction and wear behaviors

Fig. 4 describes the change of COF against sliding distance at mode 1 test. More results are shown in Fig. S4 of SI. The mean values of COF with standard deviations in steady-state stage are listed in Table 4. The variation of COF with sliding distance can be divided into two stages which are the running-in stage followed by the steady-state stage. It can be noted that there is no particular trend for the variation of duration of the running-in stage with contact pressure. For RFM and SFM, durations of running-in stage are shorter than those of the steady-state stage in most cases. While for CFM, the COF curve reaches the steady-state stage after a long period of running-in stage at mode 1 and 3 tests.

All friction materials have similar values of COF at each test mode ranging from 0.33-0.44 which are in agreement with the normal brake conditions, in which the COF is in the range of 0.3-0.6 [29]. Moreover, the COF increases firstly when the contact pressure is increased from 0.52 to 0.81 MPa, and then decreases as the contact pressure is further increased from 0.81 to 1.22 MPa. A peak value of COF is observed for all friction

materials at the contact pressure of 0.81 MPa. Straffelini et al. [47] also observed a peak value of COF when increasing the contact pressure.

The specific wear rates of RFM, SFM and CFM vary in the scope of 10^{-15} to 10^{-14} m^2/N indicating all friction materials exhibit mild wear conditions as listed in Table 4 [49, 50]. The specific wear rates at mode 1 test are lower than those at other test modes. Additionally, it can also be observed that the specific wear rate of RFM is lower than those of SFM and CFM at each friction condition and the average specific wear rates of RFM, SFM and CFM are 0.64×10^{-14}, 1.59×10^{-14} and 1.74×10^{-14} m^2/N respectively. The specific ware rates of disc range between 10^{-16} and 10^{-15} m^2/N indicating a mild wear for iron disc as listed in Table 5. The iron discs sliding against SFM and CFM have similar values of specific wear rate and they are higher than that of the iron disc sliding against RFM. The wear mechanisms for the iron disc are abrasive wear and tribo-oxidation [47]. RFM induces the mildest wear for iron disc because copper nano particles can work as solid lubricant which is similar to the function of graphite [3]. Therefore, the abrasive wear of iron disc is weakened which results in a lower specific wear rate.

The variations of pin sample temperatures are shown in Fig. 5. The pin temperature increases continuously until the end of experiment in most cases which demonstrates that the thermal equilibrium was not reached at the end of the tests. The pin temperatures measured at the end of tests are listed in Table 4 which are in the range of 30-65 ℃. The pin temperatures are in agreement with the mild wear conditions in which the brake pad temperatures are lower than 100 ℃ [51]. Moreover, it can be observed that RFM and SFM have similar pin temperatures and they are lower than that of CFM. It is because CFM induces a severer wear condition so that more heat is produced leading to a higher pin temperature compared with RFM and SFM.

3.2. Characteristics of contact surfaces

Fig. 6 shows the friction layers on the pin surface after mode 1 test. Fig. S5 of SI shows the friction layers on the pin surface after mode 2 and 3 tests. It can be observed that unconnected irregular friction layers spread over the majority of pin surface for all friction materials. After the mode 1 test, there are some cracks on the surfaces of CFM and SFM as shown in Fig. 6; while there are few cracks on the surface of RFM. From the Fig. S5 of SI, few cracks are observed on surfaces of all friction materials after mode 3

test. The friction layers on pin surfaces become larger with increasing contact pressure. In addition, SFM and CFM present smaller friction layers on their contact surfaces than RFM after modes 2 and 3 tests.

Fig. 7 and Fig. S6 of SI show the high-resolution SEM pictures of friction layers on SFM surfaces after modes 1 and 2 tests. From the EDXS analysis, the primary plateaus are formed of steel fibers and the secondary plateaus are formed of compacted wear debris as circled by black dash lines. In addition, it can also be observed that some secondary plateaus are higher than adjacent primary plateaus. Some previous studies have reported that some primary plateaus were covered by thin friction layers extended from the secondary plateaus [12, 33]. If these thin friction layers are detached from the primary plateaus, the primary plateaus are exposed with a lower height. Fig. S7 of SI shows the high-resolution pictures for the friction layers on the CFM surface after mode 2 test. It can be observed hard particles form the primary plateaus with a circular shape. In addition, a thin layer of wear debris spreads over the primary plateaus so that most ingredients in friction materials can be detected. The contact plateaus of CFM are smaller than those of SFM and RFM. It is mainly because the size of hard particles is smaller than that of metallic fibers. The hard particles enhance the abrasion wear on the pin surface and subsequently restrict the wear debris pile up against the primary plateaus which also contributes to a smaller size of contact plateaus for CFM. Fig. S8 of SI shows the high-resolution SEM pictures of friction layers on the RFM surface after mode 3 test. The friction layer with high copper content (38.11 wt%) is obviously smoother than the adjacent friction layer with low copper content (6.11 wt%). The main elemental compositions of the secondary plateaus on pin surfaces measured with EDXS point spectra are listed in Table 6. There are no special trends for elemental compositions with various contact pressures. It can be found that a lot of iron is detected which indicates that iron oxides produced from the tribo-oxidation of disc surface enter into the secondary plateaus. This phenomenon is also observed in our previous study [28] and Leonardi et al. [12].

The number-area distributions of friction layers are shown in Fig. S9 of SI. Fractal dimensions of pin surfaces are calculated from these number-area distributions as listed in Table 4. The average fractal dimensions of SFM and CFM are 2.27 and 2.29

401 respectively which are smaller than that of RFM with the value of 2.67. Moreover, there
402 is no particular trend of fractal dimension with contact pressure for all friction materials.
403 The worn surfaces of iron discs are shown in Fig. 8. A lot of grooves can be
404 observed on the worn surface of disc for all friction materials. This phenomenon indicates
405 that the abrasive wear plays an important role in the wear of a disc. In addition, as shown
406 in the black area in Fig. 8b, graphite lamellae can also be observed on the worn surface of
407 disc after sliding against SFM. This graphite lamellae emerges on the disc surface can
408 mitigate the wear condition on the disc surface [52]. Some parts of disc surface can peel
409 off due to the defects in the disc so that some pits can be observed on the disc surface
410 after test as shown in Fig. 8.

411 *3.3. Airborne wear particle emissions*

412 Particle number size distributions at mode 2 test are shown in Fig. 9. More results
413 are shown in Fig. S10 of SI. It can be observed that all friction materials have similar
414 shape of particle number size distribution and a lot of particles are in the range of 40-300
415 nm. Moreover, there are multimodal distributions at modes 2 and 3 tests. At mode 1 test,
416 no obvious peaks can be observed for all friction materials. It should be noted that a lot of
417 ultrafine particles with the diameter about 15 nm are observed at mode 1 test for all
418 friction materials.
419 Total number concentrations (TNCs) and geometric mean dimeters (GMDs)
420 measured with the SMPS are listed in Table 7. For all friction materials, TNC increases
421 with increasing the contact pressure. Generally, RFM presents the lowest TNC and SFM
422 presents the highest TNC. GMD is in the range of 70-140 nm for all friction materials
423 which is in line with results in our previous study [38]. GMD also increases with
424 increasing contact pressure in most cases. In addition, the GMD of RFM is smaller than
425 that of SFM and CFM. Wahlström et al. [41] also reported that the particle number size
426 distributions of airborne wear particles emitted from disc brakes and measured with
427 SMPS show a dominant peak around 100 nm. The particle mass concentrations (PMCs)
428 of PM_{10} are listed in Table 7. Similar to TNC results, mass concentrations also increase
429 with the increment of contact pressure for all friction materials. Moreover, RFM has the
430 lowest mass concentration of PM_{10} and SFM has the highest value of it.

3.4. Brake squeal noise

Brake squeal and vibration spectra for SFM at mode 2 test are shown in Fig. 10. More detailed results are shown in Figs. S11-S13. It can be observed that frequencies of peaks in SPL spectra are consistent with the relevant frequencies of peaks in vibration spectra for all friction materials. This phenomenon indicates that brake squeal is generated from the friction induced vibration on the contact surface. Moreover, the peaks in tangential acceleration spectra are higher than those in normal acceleration spectra at most frequencies. Especially for the peak around 2000 Hz, the tangential acceleration is obviously higher than the normal acceleration. It can be concluded that the friction induced tangential vibration has a larger contribution to the brake squeal noise than normal vibration. The A-weighted SPLs of brake squeal noise with standard deviation for all friction materials are shown in Fig. 11. The A-weighted SPL increases with increasing contact pressure for all friction materials. It is because higher contact pressure introduces more energy into the contact, and subsequently increases the fraction of energy dissipating as acoustic energy [21]. The SPLs among different friction materials are comparable. However, it can still be observed that RFM has the lowest SPL and CFM has the highest value.

4. Discussion

The formation and deterioration of friction layers on the contact surfaces determine the wear process between pin and disc [49]. It is a dynamical equilibrium process that the formation and disruption occur simultaneously at different sites on the pin sample surface [53]. Friction layers consist of two parts. The primary plateaus are formed by the ingredients with high wear resistant protruding from the pin surface, such as metallic fibers [54]. The secondary plateaus are formed by the wear debris accumulating on the primary plateaus [28]. The variation of COF is affected by the adhesion and abrasion between the contact surfaces of pin and disc [50, 55]. The adhesive interaction is closely related to the friction layer's ingredients. Since the disc is made of grey cast iron, steel and copper fibers have stronger adhesive interaction than ceramic fiber. Therefore, stronger junctions between asperities on RFM/SFM surfaces and disc surface can be built and the steady-state stage can be reached faster [56]. In addition,

Ceramic fibers contain SiO_2 and Al_2O_3 which are hard components that can facilitate the abrasive wear of contact surfaces. This enhanced abrasion improves the wear intensity between contact surfaces leading to a longer running-in stage.

The friction force is also affected by the real contact area. When increasing the contact pressure from 0.52 to 0.81 MPa, the real contact area is enlarged and then the friction force and friction coefficient are also increased. With further raising the contact pressure from 0.81 to 1.22 MPa, the friction coefficient is decreased because of the disproportional extension of real contact area which impacts the increment of friction force [56]. The normal contact pressure during vehicle braking is in the range of 1-3 MPa. On the one hand, some studies reported that the COF was increased with increasing contact pressure when the disc brake was operated under low contact pressure conditions [15, 57, 58]. On the other hand, some studies found that the COF was decreased with increasing contact pressure when the disc brake was operated under normal pressure conditions [34, 59]. If brake conditions contain both low and normal contact pressure conditions, different variation trends of COF with contact pressures can be observed.

The standard deviation (SD) of COF for RFM is lower than that for SFM and CFM. SD indicates the variation of COF in the experiments. Lower SD demonstrates a smoother friction process. It is because the soft copper nano particles can work as solid lubricant that can mitigate the wear process on the contact surfaces, and then reduce the variation of COF [3, 12]. Thus, the SD of COF for RFM is lower than those of SFM and CFM. These copper nano particles produced from the severe plastic deformation are also responsible for the lower specific wear rate of RFM compared with those of SFM and CFM. It is because the copper particles commonly own an equiaxed structure which can be incorporated into friction layers easily. These copper particles improve the strength of secondary plateaus, restrict their disruption and then reduce the specific wear rate [3, 60]. The higher specific wear rate of CFM is also because of the SiO_2 and Al_2O_3 contents which are generated from the wear of the ceramic fiber in CFM. SiO_2 and Al_2O_3 are hard abrasive particles that can aggravate the abrasive wear of friction materials leading to a higher specific wear rate.

The effect of copper nano particles leads to the absence of cracks on the surfaces of RFM as shown in Fig. 6a. In contrast, the absence of copper in SFM and CFM is

responsible for the cracks on the friction layers of SFM and CFM surfaces as shown in Figs. 6b and 6c. The CFM surface exhibits the most cracks in all the friction materials which is in line with the largest average specific wear rate of CFM. These two observations indicate that the CFM induces the severest wear condition on the contact surface of the pin sample. With increasing contact pressure, compactness of friction layers is improved so that most cracks disappeared in the mode 3 test. Cracks on the friction layers also indicate the weaker binding force between friction layers and bulk material for SFM and CFM compared with that for RFM [44]. The binding force between friction layers and bulk material affect the generation process of airborne particles which will be discussed later. Leonardi et al. [12] also observed that the lack of copper introduced some cracks on the pin surface. From the EDXS analysis shown and not yet shown in this paper, only a small fraction of primary plateaus is detected for all friction materials because the majority of primary plateaus are covered by a thin film of wear debris. Similar phenomenon was also observed by Österle et al. [61] who stated that the brake pad and disc were separated by a layer of third body consisting of non-crystalline wear debris and coarse wear particles with a thickness of about 10 μm.

Fractal dimension, as a parameter representing the surface roughness, is determined by the formation and disruption of friction layers on the contact surface. The majority of primary plateaus are covered by a thin film of wear debris which is extended from the adjacent primary plateaus. Thus, the shape and size of the friction layers measured by SEM on the worn pin surface depend on the compactness and wear resistant of secondary plateaus and the thin film of wear debris above the primary plateaus. Since the copper nano particles can improve the wear resistant, RFM has a larger fractal dimension than SFM and CFM. The comparable fractal dimensions between SFM and CFM indicate the surface roughness of these two friction materials is comparable which is consistent with the observed morphologies of the contact surface that there are cracks on the friction layers of SFM and CFM surfaces, while no cracks on the friction layers of RFM surface. Since fraction dimension is evaluated from the number-area distribution of the friction layers, a small fractal dimension value indicates a low variation of friction layer size. In present study, the size variations of friction layers on the SFM and CFM surfaces are lower than that on the RFM surface. This phenomenon affects the local

oscillation on the brake pad surface leading to various brake squeal noise emissions which will be discussed later.

The elemental compositions of airborne wear particles emitted from disc brakes have been investigated through similar pin-on-disc test-rig in some previous studies [33, 62]. They reported that the main element of particles is iron, and the majority of particles are produced from the tribo-oxidation and abrasion of the iron disc. The tribo-oxidation of iron disc is independent from the friction materials. Therefore, all friction materials have a similar shape for particle number size distributions and a similar size range of airborne particles. With increasing contact pressure, these two wear mechanisms are enhanced leading to a higher particle emission. As introduced before, copper nano particles can work as solid lubricant. Therefore, they can mitigate the abrasion on disc surface leading to lower particle emission results of RFM compared with those of SFM and CFM. The steel fiber in SFM can also produce some iron particles under abrasion wear. Therefore, SFM sliding against iron disc produces higher particle emissions than CFM. Some particles are generated from the disruption of friction layers which have a flaky shape with large particle diameter [33, 62, 63]. As introduced above, friction layers with some cracks exhibited a weaker binding force between friction layers and bulk material. Therefore, more friction layers on the surfaces of SFM and CFM are disrupted and emitted into the surrounding environment as airborne particles compared with those on the surface of RFM. This phenomenon leads to the smaller GMD of RFM particles compared with that of SFM and CFM particles. The various formation mechanisms of airborne wear particles result in the multi-peaks in the particle number size distribution. Contact pressure is the driving force for the particle agglomeration at the interface [64]. Larger contact pressure can promote the agglomeration process of particles leading to a larger particle size. It should be noted that the SD of particle mass concentration is very high which can be larger than 50% of the mean values as listed in Table 7. The very high SD indicates that the particle generation process varies heavily even though the COF curve keeps stable with low SD.

The SPL spectra are quite different among different friction materials under the same friction condition. This is because the brake squeal is very sensitive to the friction process. Small variations in contact temperature and friction coefficient can result in

554 different squeal propensities or frequencies [65]. As shown in Figs. 4 and 5, the friction
555 coefficient and pin temperature vary continuously during the whole friction process and
556 the variation curves are different among various friction materials. Thus, SPL spectra
557 among different friction materials are quite different. The lowest SPL of RFM can be
558 attributed to the following two factors. Firstly, the lubricant effect of copper nano
559 particles which can reduce the vibration on the contact surfaces leading to a lower SPL
560 [3]. Secondly, the size variations of friction layers on the SFM and CFM surfaces are
561 lower than that on the RFM surface. The size of a friction layer affects the amplitude and
562 frequency of local oscillation, and then influences the brake squeal noise. Low variation
563 of friction layer size leads to the synchronized oscillation of the friction layers on the
564 contact surface and subsequently increases the amplitude of total local oscillation [27].
565 From the acceleration spectra, several peaks are observed at very high frequencies (6000-
566 10000 Hz). These high frequency vibrations at tangential and normal directions indicate
567 the local contact stresses on the friction layers also oscillate largely at tangential and
568 normal directions. The large oscillations of local contact stresses are also responsible for
569 the cracks on the brake pad surface as shown in Fig. 6.

570 **5. Conclusions**

571 Two copper-free friction materials, SFM and CFM, were manufactured by
572 replacing the copper fiber in a NAO friction material (RFM) with steel fiber and ceramic
573 fiber respectively. A pin-on-disc test-rig was employed to investigate the friction and
574 wear behaviors, characteristics of contact surfaces, airborne wear particle emissions and
575 brake squeal noise of these three friction materials sliding against an iron disc. The
576 results can be concluded as follows:

577 1. All friction materials have comparable values of COF at the steady-state stage.
578 The specific wear rate of RFM is lower than those of SFM and CFM. SFM and
579 CFM have similar values of specific wear rate.
580 2. Contact plateaus on SFM and CFM surfaces have more cracks than those on the
581 contact surface of RFM. But there are no cracks on the friction layers under the
582 largest contact pressure for all friction materials. Fractal dimensions vary from

2.22 to 2.77 for all friction materials and RFM has larger fractal dimension than SFM and CFM.

3. There are multimodal distributions for the particle number size distribution of airborne wear particles. SFM and CFM have higher particle emissions and larger particle size than RFM.
4. Brake squeal noise is mainly caused by the friction induced tangential vibration. The A-weighted brake squeal noise among different friction materials are comparable.

The encouraging outcomes are all friction materials exhibit comparable friction coefficients and have similar A-weight SPLs of brake squeal noise. But the airborne particle emissions of SFM and CFM are higher than those of RFM. Results show that more cracks on the friction layers result in higher particle emissions. Further study should be conducted to modify the friction material formulation to improve the friction layer's quality and reduce the airborne wear particle emissions.

The present study was conducted under the mild wear conditions with low friction material temperature. However, copper fibers have good tribology performance under severe wear conditions with high friction material temperature. A future study is also necessary to compare the tribology performances, airborne wear particle emissions and brake squeal noise among RFM, SFM and CFM under the severe wear conditions.

Acknowledgement

Authors would like to thank The Hong Kong Polytechnic University for the financial support (RUTT).

References

[1] Xiao XM, Yin Y, Bao JS, Lu LJ, Feng XJ. Review on the friction and wear of brake materials. Advances in Mechanical Engineering. 2016;8:1687814016647300.

[2] Lee PW, Filip P. Friction and wear of Cu-free and Sb-free environmental friendly automotive brake materials. Wear. 2013;302:1404-13.

[3] Österle W, Prietzel C, Kloß H, Dmitriev AI. On the role of copper in brake friction materials. Tribol Int. 2010;43:2317-26.

[4] Bijwe J, Kumar M, Gurunath PV, Desplanques Y, Degallaix Ge. Optimization of brass contents for best combination of tribo-performance and thermal conductivity of non-asbestos organic (NAO) friction composites. Wear. 2008;265:699-712.
[5] Ho SC, Chern Lin JH, Ju CP. Effect of fiber addition on mechanical and tribological properties of a copper/phenolic-based friction material. Wear. 2005;258:861-9.
[6] Barros LY, Poletto JC, Neis PD, Ferreira NF, Pereira CHS. Influence of copper on automotive brake performance. Wear. 2019;426-427:741-9.
[7] Kumar M, Bijwe J. Non-asbestos organic (NAO) friction composites: Role of copper; its shape and amount. Wear. 2011;270:269-80.
[8] Agency EP. Memorandum of Understanding on Copper Mitigation in Watersheds & Waterways. <https://www.epa.gov/sites/production/files/2015-11/documents/copper_brakepads_mou.pdf>. 2015.
[9] Straffelini G, Ciudin R, Ciotti A, Gialanella S. Present knowledge and perspectives on the role of copper in brake materials and related environmental issues: A critical assessment. Environ Pollut. 2015;207:211-9.
[10] Sandahl JF, Baldwin DH, Jenkins JJ, Scholz NL. A Sensory System at the Interface between Urban Stormwater Runoff and Salmon Survival. Environ Sci Technol. 2007;41:2998-3004.
[11] Beyers DW, Farmer MS. Effects of copper on olfaction of colorado pikeminnow. Environ Toxicol Chem. 2001;20:907-12.
[12] Leonardi M, Menapace C, Matejka V, Gialanella S, Straffelini G. Pin-on-disc investigation on copper-free friction materials dry sliding against cast iron. Tribol Int. 2018;119:73-81.
[13] Menapace C, Leonardi M, Matějka V, Gialanella S, Straffelini G. Dry sliding behavior and friction layer formation in copper-free barite containing friction materials. Wear. 2018;398-399:191-200.
[14] Mahale V, Bijwe J, Sinha S. A step towards replacing copper in brake-pads by using stainless steel swarf. Wear. 2019;424:133-42.
[15] Jang H, Ko K, Kim SJ, Basch RH, Fash JW. The effect of metal fibers on the friction performance of automotive brake friction materials. Wear. 2004;256:406-14.
[16] Kumar M, Bijwe J. Optimized selection of metallic fillers for best combination of performance properties of friction materials: A comprehensive study. Wear. 2013;303:569-83.
[17] Grigoratos T, Martini G. Brake wear particle emissions: a review. Environ Sci Pollut Res. 2015;22:2491-504.
[18] Nosko O, Olofsson U. Effective density of airborne wear particles from car brake materials. J Aerosol Sci. 2017;107:94-106.
[19] Lyu Y, Leonardi M, Wahlström J, Gialanella S, Olofsson U. Friction, wear and airborne particle emission from Cu-free brake materials. Tribol Int. 2020;141:105959.
[20] Yang M, Afaneh A-H, Blaschke P. A Study of Disc Brake High Frequency Squeals and Disc In-Plane/Out-of-Plane Modes. SAE International; 2003.

[21] Lazzari A, Tonazzi D, Massi F. Squeal propensity characterization of brake lining materials through friction noise measurements. Mech Syst Sig Process. 2019;128:216-28.
[22] Kchaou M, Mat Lazim AR, Abu Bakar AR, Fajoui J, Elleuch R, Jacquemin F. Effects of Steel Fibers and Surface Roughness on Squealing Behavior of Friction Materials. Trans Indian Inst Met. 2016;69:1277-87.
[23] Di Bartolomeo M, Massi F, Baillet L, Culla A, Fregolent A, Berthier Y. Wave and rupture propagation at frictional bimaterial sliding interfaces: From local to global dynamics, from stick-slip to continuous sliding. Tribol Int. 2012;52:117-31.
[24] Godet M. The third-body approach: A mechanical view of wear. Wear. 1984;100:437-52.
[25] Guangxiong C, Zhongrong Z, Kapsa P, Vincent L. Effect of surface topography on formation of squeal under reciprocating sliding. Wear. 2002;253:411-23.
[26] Eriksson M, Bergman F, Jacobson S. Surface characterisation of brake pads after running under silent and squealing conditions. Wear. 1999;232:163-7.
[27] Lee S, Jang H. Effect of plateau distribution on friction instability of brake friction materials. Wear. 2018;400-401:1-9.
[28] Wei L, Choy YS, Cheung CS. A study of brake contact pairs under different friction conditions with respect to characteristics of brake pad surfaces. Tribol Int. 2019;138:99-110.
[29] Federici M, Gialanella S, Leonardi M, Perricone G, Straffelini G. A preliminary investigation on the use of the pin-on-disc test to simulate off-brake friction and wear characteristics of friction materials. Wear. 2018;410-411:202-9.
[30] Patnaik A, Kumar M, Satapathy BK, Tomar BS. Performance sensitivity of hybrid phenolic composites in friction braking: Effect of ceramic and aramid fibre combination. Wear. 2010;269:891-9.
[31] Kim SJ, Jang H. Friction and wear of friction materials containing two different phenolic resins reinforced with aramid pulp. Tribol Int. 2000;33:477-84.
[32] Wahlström J, Gventsadze D, Olander L, Kutelia E, Gventsadze L, Tsurtsumia O, et al. A pin-on-disc investigation of novel nanoporous composite-based and conventional brake pad materials focussing on airborne wear particles. Tribol Int. 2011;44:1838-43.
[33] Alemani M, Gialanella S, Straffelini G, Ciudin R, Olofsson U, Perricone G, et al. Dry sliding of a low steel friction material against cast iron at different loads: Characterization of the friction layer and wear debris. Wear. 2017;376-377:1450-9.
[34] Wahlström J, Matějka V, Lyu Y, Söderberg A. Contact Pressure and Sliding Velocity Maps of the Friction, Wear and Emission from a Low-Metallic/Cast-Iron Disc Brake Contact Pair. Tribology in Industry. 2017;39.
[35] Komvopoulos K, Ye N. Three-dimensional contact analysis of elastic-plastic layered media with fractal surface topographies. J Tribol. 2001;123:632-40.
[36] Thomas TR, Rosén BG, Amini N. Fractal characterisation of the anisotropy of rough surfaces. Wear. 1999;232:41-50.
[37] Majumdar A, Bhushan B. Role of Fractal Geometry in Roughness Characterization and Contact Mechanics of Surfaces. J Tribol. 1990;112:205-16.

[38] Wei L, Choy YS, Cheung CS. A study of brake contact pairs under different brake conditions with respect to airborne wear particle emissions. Eurobrake 2019. Dresden, German2019.
[39] Nosko O, Vanhanen J, Olofsson U. Emission of 1.3–10 nm airborne particles from brake materials. Aerosol Sci Technol. 2016;51:91-6.
[40] Nosko O, Olofsson U. Quantification of ultrafine airborne particulate matter generated by the wear of car brake materials. Wear. 2017;374-375:92-6.
[41] Wahlström J, Söderberg A, Olander L, Jansson A, Olofsson U. A pin-on-disc simulation of airborne wear particles from disc brakes. Wear. 2010;268:763-9.
[42] Wahlström J, Söderberg A, Olander L, Olofsson U, Jansson A. Airborne wear particles from passenger car disc brakes: A comparison of measurements from field tests, a disc brake assembly test stand, and a pin-on-disc machine. Proceedings of the Institution of Mechanical Engineers, Part J: Journal of Engineering Tribology. 2009;224:179-88.
[43] Perricone G, Wahlstro m J, Olofsson U. Towards a test stand for standardized measurements of the brake emissions. Proceedings of the Institution of Mechanical Engineers, Part D: Journal of Automobile Engineering. 2015;230:1521-8.
[44] Massi F, Berthier Y, Baillet L. Contact surface topography and system dynamics of brake squeal. Wear. 2008;265:1784-92.
[45] Disc and Drum Brake Dynamometer Squeal Noise Matrix. SAE International; 2006.
[46] Moore S, Lai J, Oberst S, Papinniemi A, Hamdi S, Stanef D. Determining the effect of pad lining geometry on brake noise performance. INTER-NOISE and NOISE-CON Congress and Conference Proceedings: Institute of Noise Control Engineering; 2008. p. 3132-48.
[47] Straffelini G, Maines L. The relationship between wear of semimetallic friction materials and pearlitic cast iron in dry sliding. Wear. 2013;307:75-80.
[48] Moffat RJ. Describing the uncertainties in experimental results. Exp Therm Fluid Sci. 1988;1:3-17.
[49] Chandra Verma P, Menapace L, Bonfanti A, Ciudin R, Gialanella S, Straffelini G. Braking pad-disc system: Wear mechanisms and formation of wear fragments. Wear. 2015;322-323:251-8.
[50] Federici M, Menapace C, Moscatelli A, Gialanella S, Straffelini G. Pin-on-disc study of a friction material dry sliding against HVOF coated discs at room temperature and 300 °C. Tribol Int. 2017;115:89-99.
[51] Straffelini G, Verlinski S, Verma PC, Valota G, Gialanella S. Wear and Contact Temperature Evolution in Pin-on-Disc Tribotesting of Low-Metallic Friction Material Sliding Against Pearlitic Cast Iron. Tribol Lett. 2016;62:36.
[52] Straffelini G, Pellizzari M, Maines L. Effect of sliding speed and contact pressure on the oxidative wear of austempered ductile iron. Wear. 2011;270:714-9.
[53] Österle W, Urban I. Friction layers and friction films on PMC brake pads. Wear. 2004;257:215-26.
[54] Eriksson M, Jacobson S. Tribological surfaces of organic brake pads. Tribol Int. 2000;33:817-27.

[55] Straffelini G, Pellizzari M, Molinari A. Influence of load and temperature on the dry sliding behaviour of Al-based metal-matrix-composites against friction material. Wear. 2004;256:754-63.
[56] Straffelini G. Friction and wear: methodologies for design and control: Springer; 2015.
[57] Wahlström J, Olander L, Olofsson U. A Pin-on-Disc Study Focusing on How Different Load Levels Affect the Concentration and Size Distribution of Airborne Wear Particles from the Disc Brake Materials. Tribol Lett. 2012;46:195-204.
[58] Bode K, Schramm T, Perzborn N, Raczek S, Münchhoff J, Ostermeyer G-P. LOW μ AT LOW PRESSURE – POTENTIAL FOR REDUCING RESIDUAL DRAG? EuroBrake 2014. Lille, France2014.
[59] Kumar M, Bijwe J. Composite friction materials based on metallic fillers: Sensitivity of μ to operating variables. Tribol Int. 2011;44:106-13.
[60] Zhang YS, Han Z, Wang K, Lu K. Friction and wear behaviors of nanocrystalline surface layer of pure copper. Wear. 2006;260:942-8.
[61] Österle W, Dörfel I, Prietzel C, Rooch H, Cristol-Bulthé AL, Degallaix G, et al. A comprehensive microscopic study of third body formation at the interface between a brake pad and brake disc during the final stage of a pin-on-disc test. Wear. 2009;267:781-8.
[62] Wahlström J, Olander L, Olofsson U. Size, Shape, and Elemental Composition of Airborne Wear Particles from Disc Brake Materials. Tribol Lett. 2010;38:15-24.
[63] Nosko O, Borrajo-Pelaez R, Hedström P, Olofsson U. Porosity and shape of airborne wear microparticles generated by sliding contact between a low-metallic friction material and a cast iron. J Aerosol Sci. 2017;113:130-40.
[64] Mosleh M, Blau PJ, Dumitrescu D. Characteristics and morphology of wear particles from laboratory testing of disk brake materials. Wear. 2004;256:1128-34.
[65] Papinniemi A, Lai JCS, Zhao J, Loader L. Brake squeal: a literature review. Applied Acoustics. 2002;63:391-400.

Tribology performance, airborne particle emissions and brake squeal noise of copper-free friction materials

L. Wei, Y.S. Choy*, C.S. Cheung, D. Jin

Department of Mechanical Engineering, The Hong Kong Polytechnic University, Hung Hom, Kowloon, Hong Kong

*Corresponding author.

Tel: +852 2766 7813

Email: mmyschoy@polyu.edu.hk

Figures

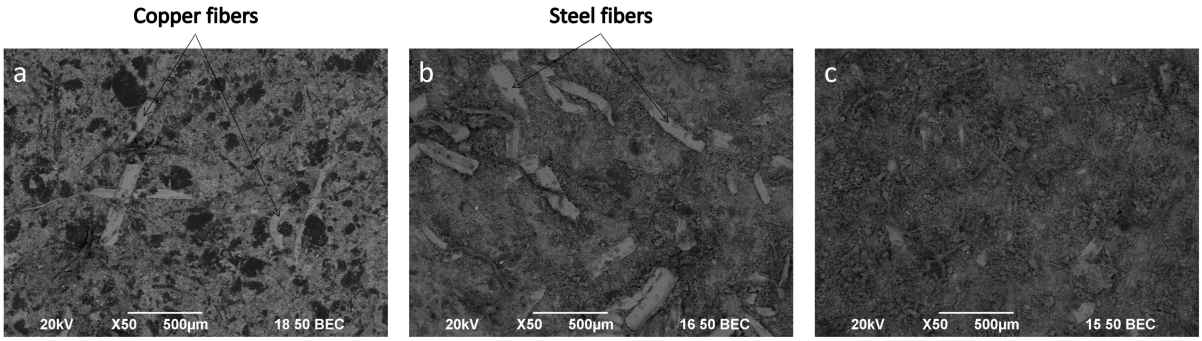

Fig. 1. BSE-SEM pictures of pin samples (a: RFM, b: SFM, c: CFM)

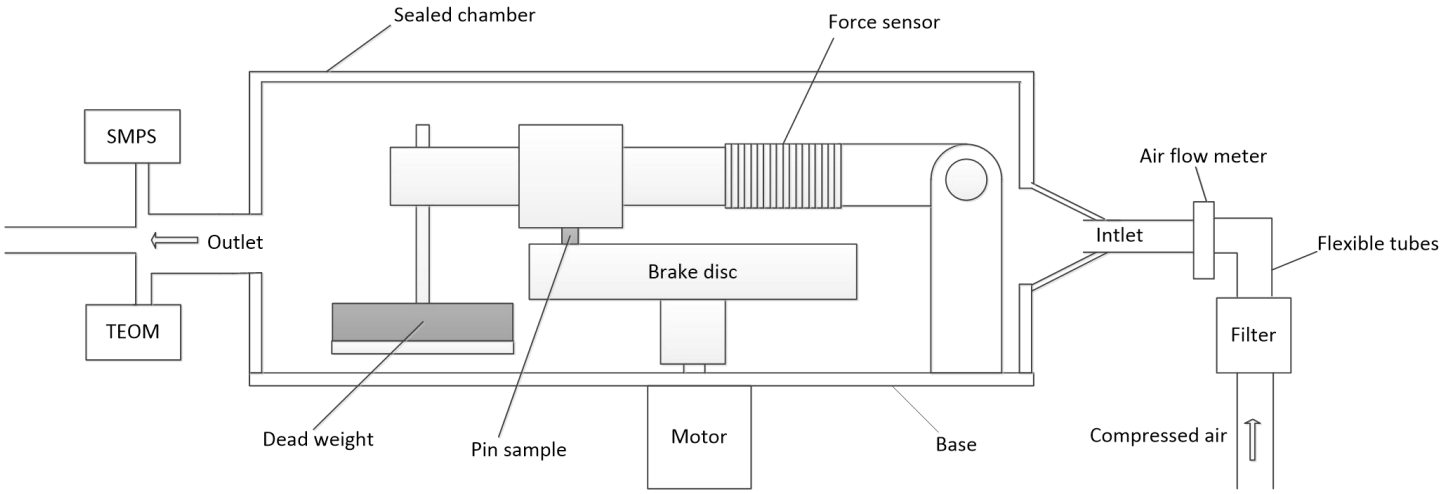

Fig. 2. Schematic of test-rig for tribology performance and airborne particle emissions

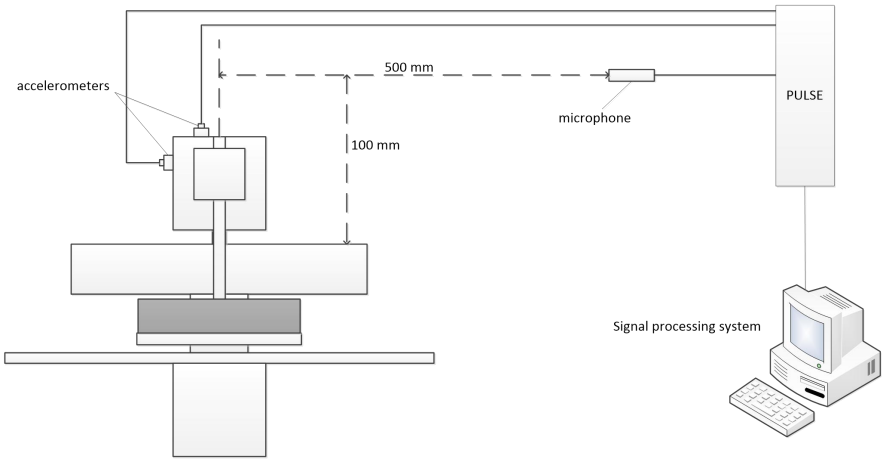

Fig. 3 Schematic of test-rig for brake squeal noise

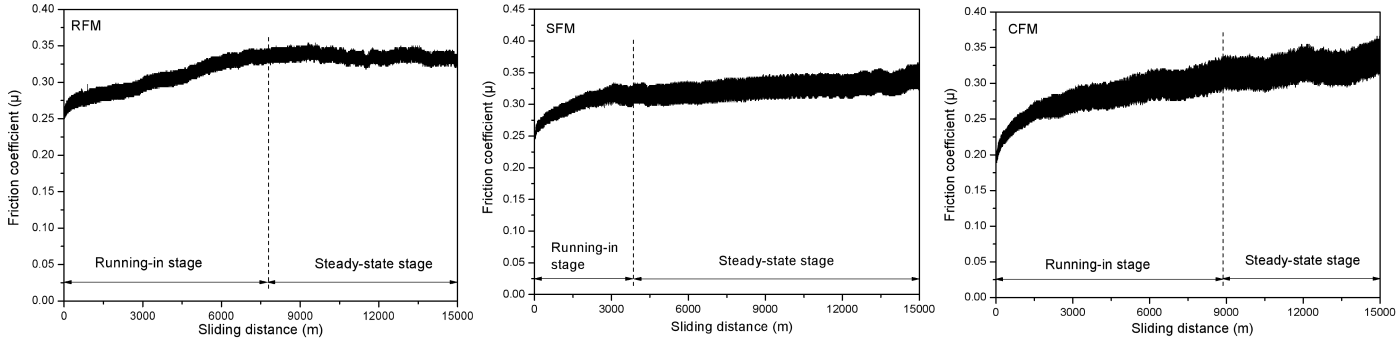

Fig. 4. Variation of friction coefficient during test (Test mode 1)

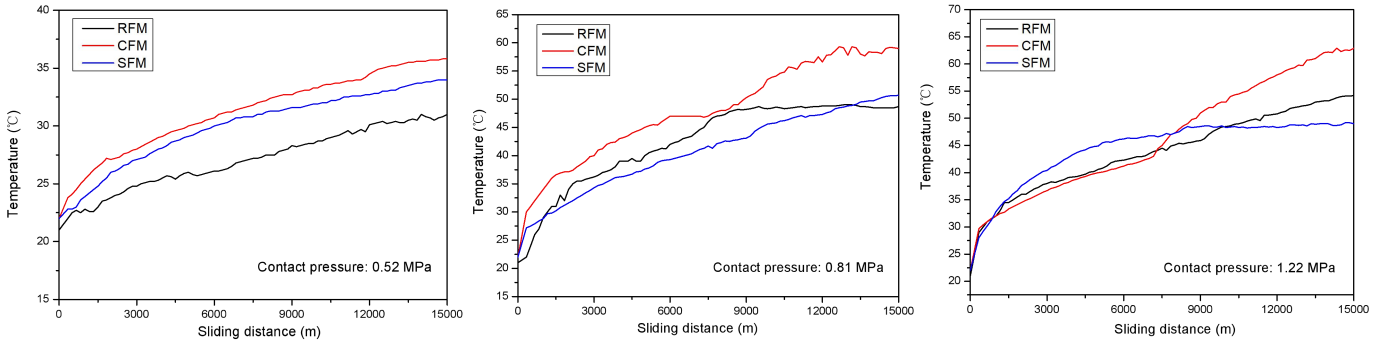

Fig. 5. Variation of pin temperature with sliding distance

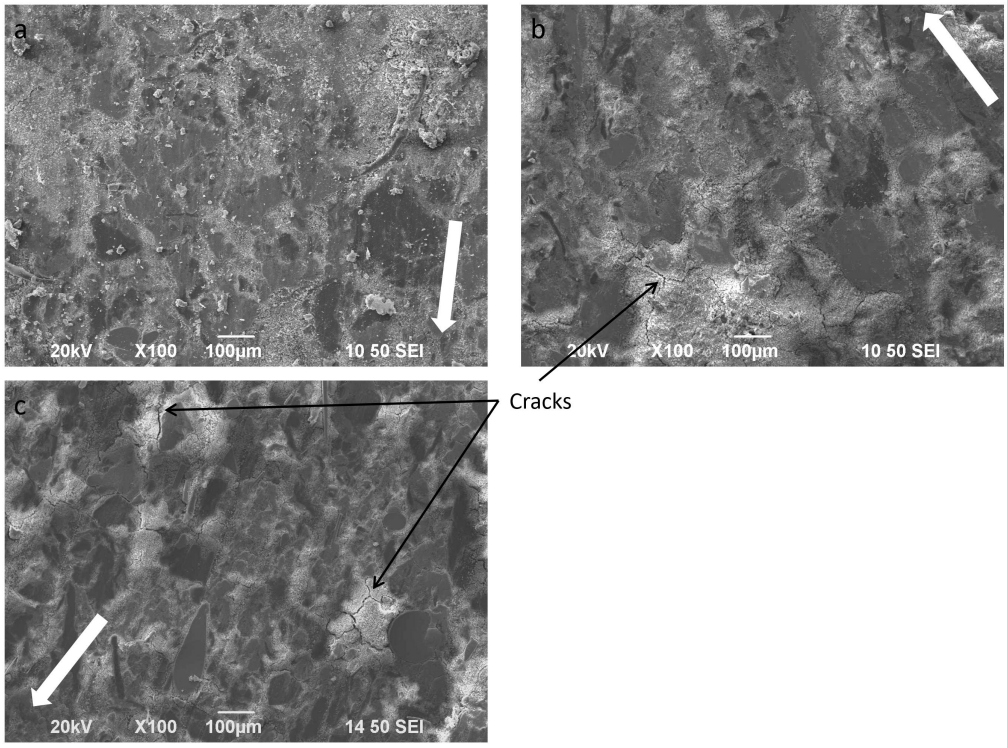

Fig. 6. SEM pictures of pin surfaces after mode 1 test (a: RFM, b: SFM, c: CFM; white arrow indicating the sliding direction).

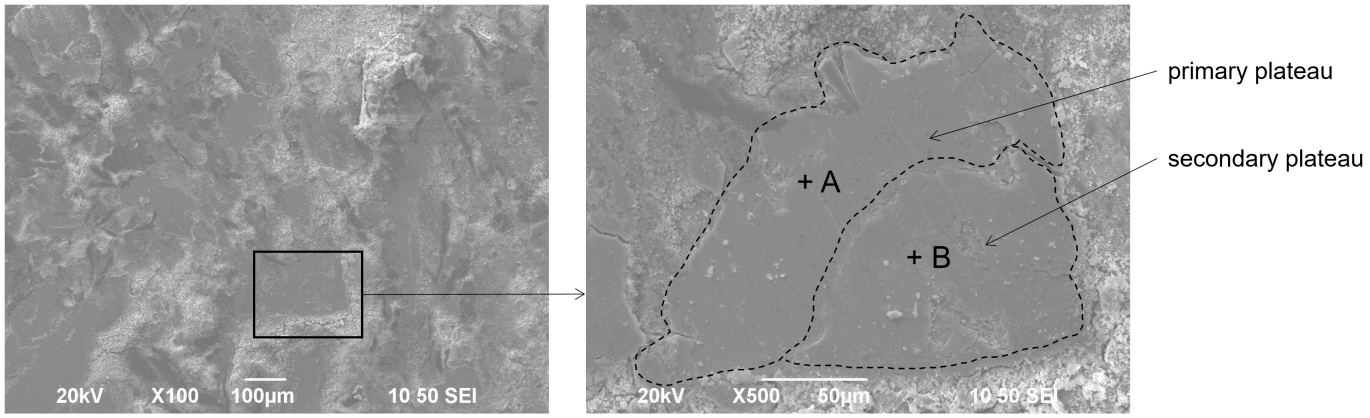

Spectrum A

Element	Weight%	Atomic%
Fe K	100.00	100.00
Totals	100.00	

Spectrum B

Element	Weight%	Atomic%
O K	25.20	55.78
Si K	3.06	3.86
S K	0.90	0.99
Ca K	1.57	1.39
Fe K	53.46	33.90
Ba L	15.81	4.08
Totals	100.00	

Fig. 7. SEM pictures and EDXS point spectra of the SFM surface (Test mode 1)

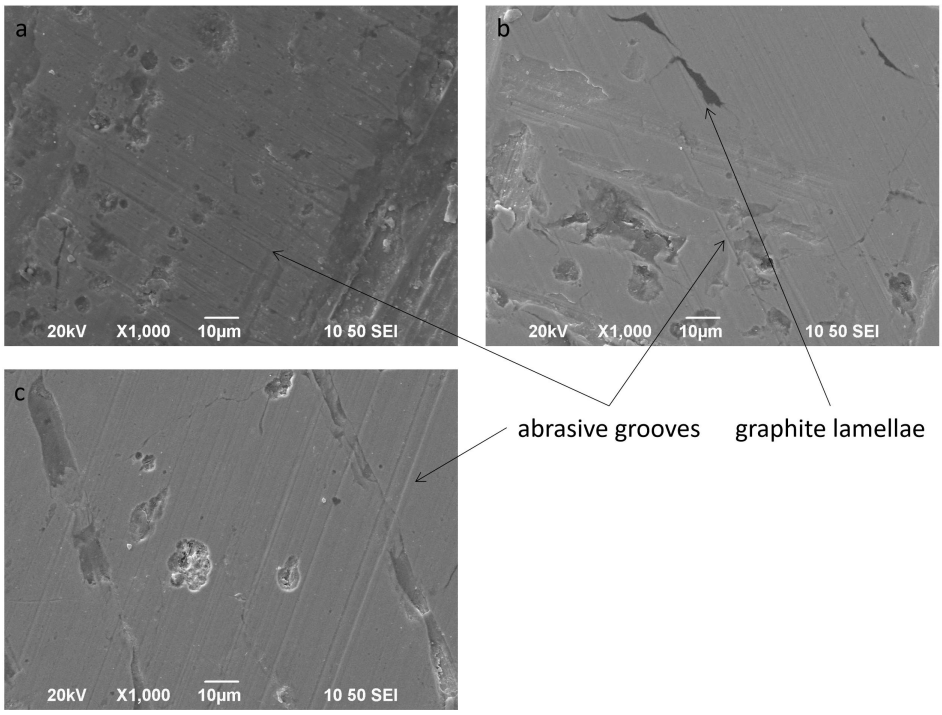

Fig. 8. SEM pictures of the worn surfaces of iron discs (a: RFM, b: SFM, c: CFM).

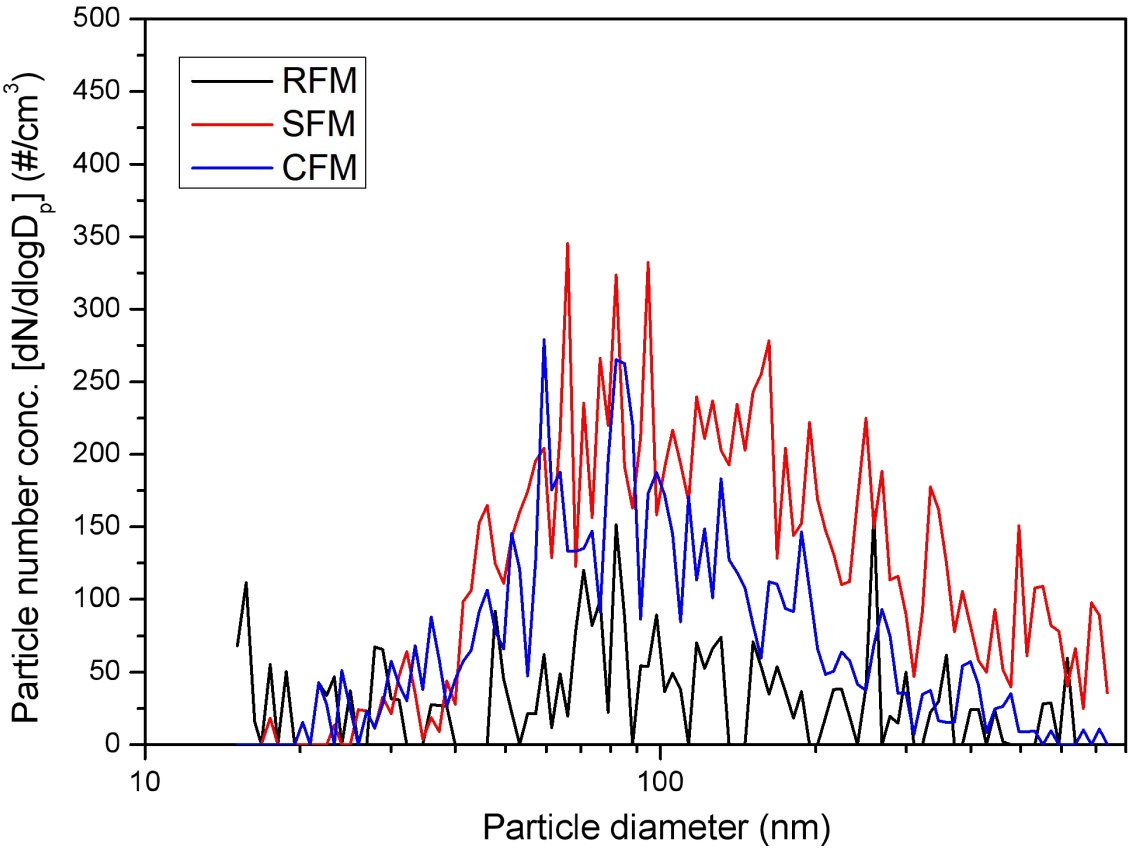

Fig. 9. Particle number size distributions at mode 2 test

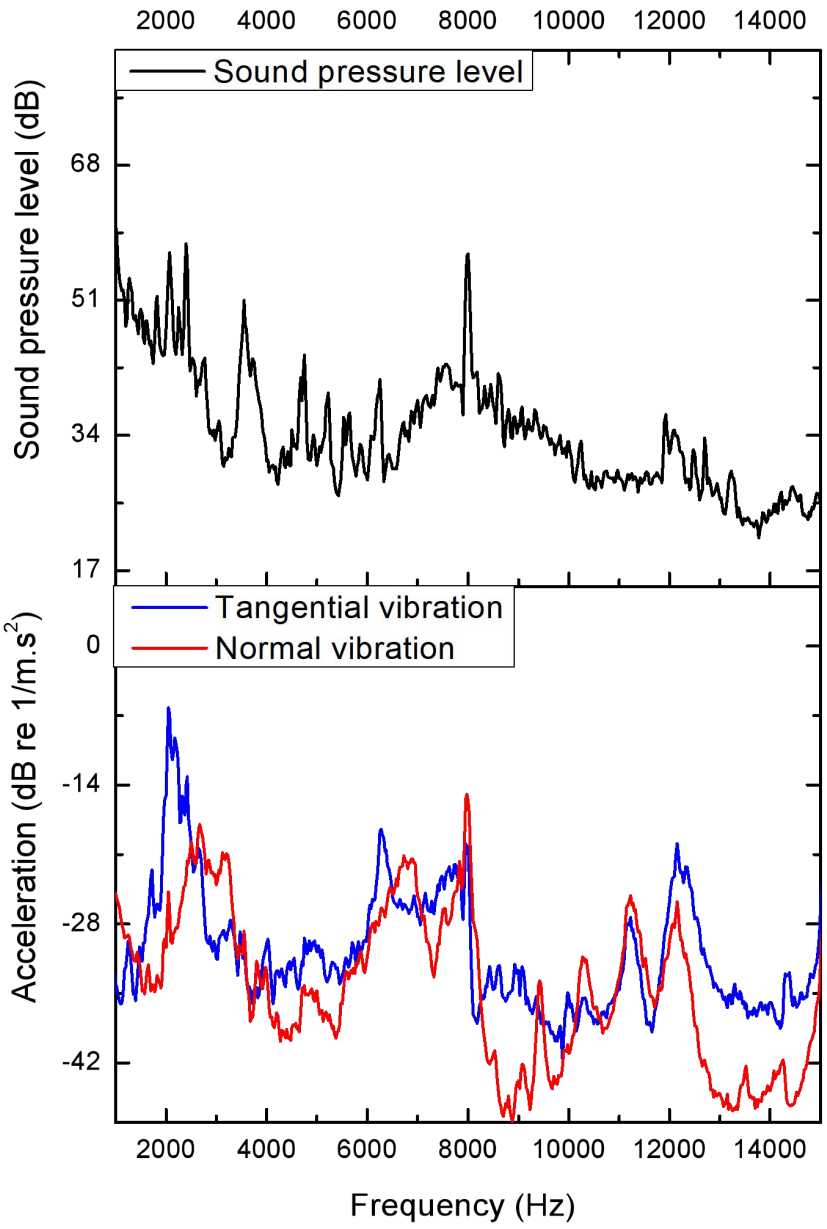

Fig. 10. SPL and acceleration spectra for SFM at mode 2 test

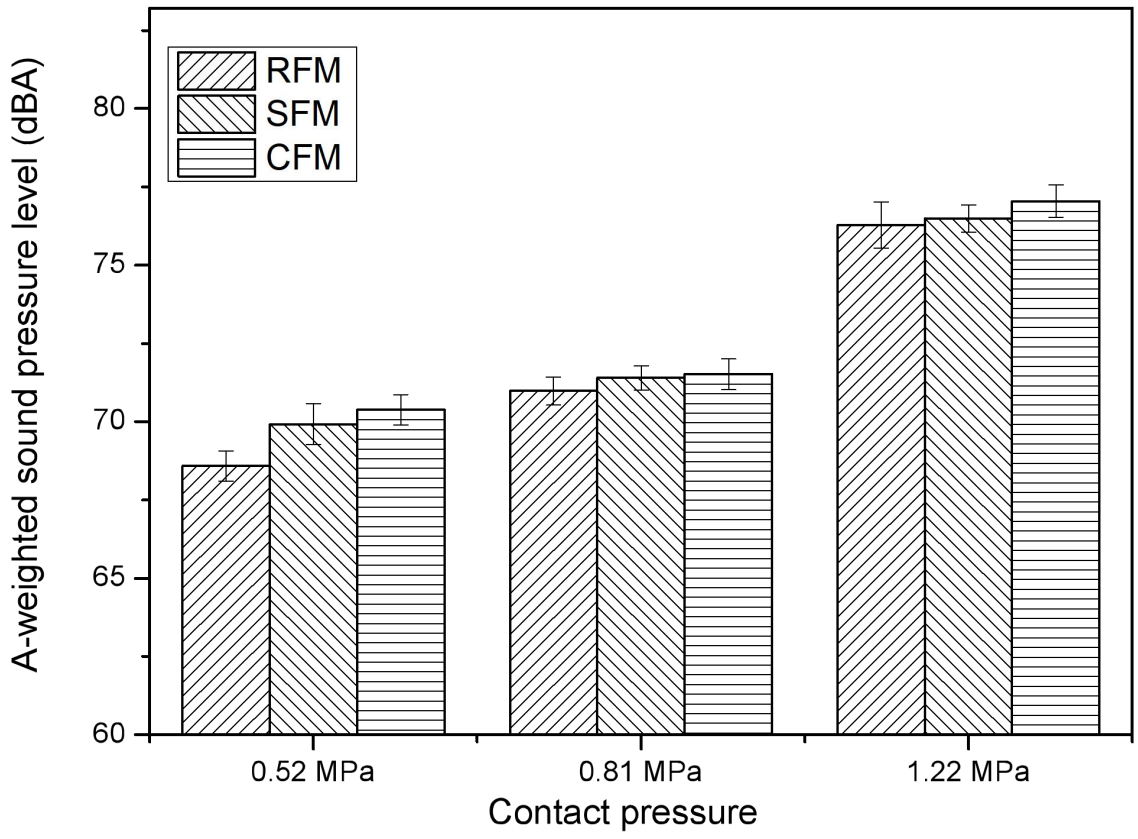

Fig. 11. A-weighted sound pressure level

Tribology performance, airborne particle emissions and brake squeal noise of copper-free friction materials

L. Wei, Y.S. Choy*, C.S. Cheung, D. Jin

Department of Mechanical Engineering, The Hong Kong Polytechnic University, Hung Hom, Kowloon, Hong Kong

*Corresponding author.

Tel: +852 2766 7813

Email: mmyschoy@polyu.edu.hk

Tables

Table 1 Specification of fibers (Supplier's data)

Physical properties	Steel fiber	Ceramic fiber	Copper fiber
Color	Sliver	White	Yellow
Diameter (μm)	100-250	4-10	150-250
Length (mm)	1-3	0.3-0.5	1-3
Density (g/cm^3)	7.85	1.95	8.94
Melting point (°C)	1538	>1200	1083
Tensile strength (MPa)	440	1400-1600	333
Purity	>98%	>98%	>98%

Ceramic fiber ingredients (vol.): SiO_2: 53-57%, Al_2O_3: 43-47%, Fe_2O_3: Trace, TiO_2: Trace, Na_2O_3: <0.5%, Alkali: Trace.

Table 2 Friction material compositions

Ingredients (vol%)	RFM	SFM	CFM
Copper fiber	10	-	-
Steel fiber	-	10	-
Ceramic fiber	-	-	10
Parent composition	90	90	90
Density (g/cm^3)	2.08±0.08	2.10±0.10	1.72±0.03

Table 3 Standard errors of results with 95% confidence level

Parameters	Standard error (%)	Parameters	Standard error (%)
Friction coefficient	3.3	Fractal dimension	1.7
Specific wear rate of friction materials	2.9	Total number concentration	4.6
Specific wear rate of disc	2.5	Particle mass concentration	6.3
Pin sample temperature	3.7	Geometric mean diameter	2.3

Table 4 Friction and wear behaviors of different friction materials

Type of friction material	Test mode	v	F_N	μ (SD)	Δm (SD)	k_s (SD)	T	D_s
	#	m/s	N	-	10^{-2}g	$10^{-14}m^2/N$	℃	-
RFM	1	2.8	52	0.335(0.008)	0.75(0.023)	0.45(0.012)	31.0	2.59
	2	2.8	81	0.434(0.010)	0.99(0.026)	0.53(0.014)	48.7	2.77
	3	2.8	122	0.359(0.007)	3.44(0.077)	0.94(0.021)	54.0	2.65
SFM	1	2.8	52	0.337(0.019)	1.46(0.031)	0.89(0.019)	34.0	2.25
	2	2.8	81	0.439(0.022)	5.33(0.098)	2.49(0.046)	49.0	2.22
	3	2.8	122	0.385(0.010)	6.24(0.14)	1.40(0.032)	50.7	2.35
CFM	1	2.8	52	0.332(0.022)	1.94(0.039)	1.44(0.029)	35.8	2.33
	2	2.8	81	0.438(0.023)	3.00(0.069)	1.62(0.037)	59.0	2.23
	3	2.8	122	0.384(0.008)	5.64(0.11)	2.15(0.041)	62.9	2.31

SD refers to standard deviation

Table 5 Specific wear rates of the discs

Type of friction material	v	F_N	k_s
	m/s	N	$10^{-15}m^2/N$
RFM	2.8	122	0.95
SFM	2.8	122	1.43
CFM	2.8	122	1.37

Table 6 Elemental compositions (wt%) of the secondary plateaus on the pin surface (Carbon and oxygen are not quantified)

(a) RFM

Element	0.52 MPa	0.81 MPa	1.22 MPa
Si	2.64	6.06	6.03
S	2.25	4.29	4.11
Ca	1.59	2.75	2.01
Fe	16.47	12.63	15.70
Cu	2.28	4.27	15.07
Ba	17.41	24.10	21.43

(b) SFM

Element	0.52 MPa	0.81 MPa	1.22 MPa
Si	3.42	4.71	3.20
S	1.69	2.52	4.76
Ca	1.33	1.42	1.49
Fe	25.26	34.88	21.91
Ba	13.11	18.32	33.52

(c) CFM

Element	0.52 MPa	0.81 MPa	1.22 MPa
Si	3.52	7.56	2.94
S	3.43	1.69	9.53
Ca	4.44	7.30	6.49
Fe	12.81	15.50	10.85
Ba	19.43	13.41	50.07

Table 7 TNC, GMD and PMC

Type of friction material	Test mode	TNC (SD)	GMD (SD)	PMC (SD)
	#	#/cm^3	nm	μg/m^3
RFM	1	36.4(0.51)	71.8(2.47)	59.8(30.57)
	2	55.9(1.43)	87.3(2.58)	119.7(75.73)
	3	121.4(1.40)	117.0(2.18)	309.5(52.41)
SFM	1	95.9(1.14)	98.9(2.56)	100.6(65.13)
	2	200.7(3.36)	133.5(2.14)	310.9(99.01)
	3	411.4(1.66)	108.6(2.05)	957.4(123.60)
CFM	1	55.1(0.95)	94.1(2.34)	90.7(55.81)
	2	119.4(1.72)	98.5(1.95)	187.7(121.90)
	3	427.7(2.02)	117.5(2.07)	474.1(127.75)

SD refers to standard deviation

Tribology performance, airborne particle emissions and brake squeal noise of copper-free friction materials

L. Wei, Y.S. Choy*, C.S. Cheung, D. Jin

Department of Mechanical Engineering, The Hong Kong Polytechnic University, Hung Hom, Kowloon, Hong Kong

*Corresponding author.

Tel: +852 2766 7813

Email: mmyschoy@polyu.edu.hk

Figures

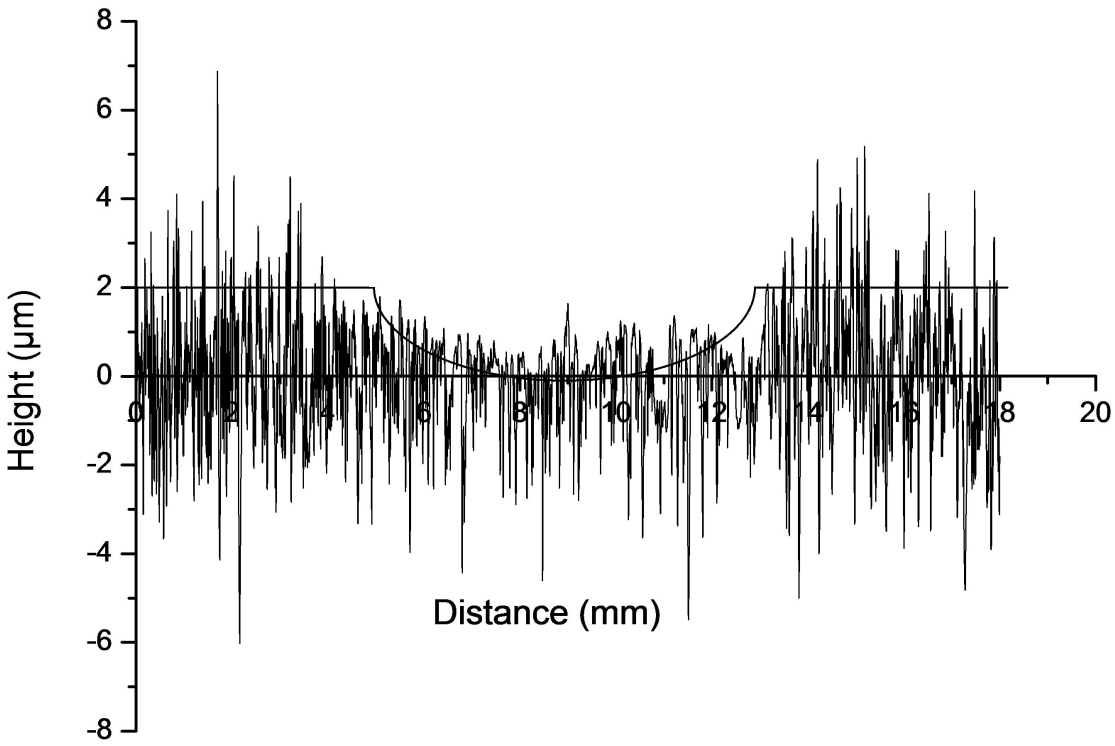

Fig. S1. Transverse surface profile of the wear track on disc sample

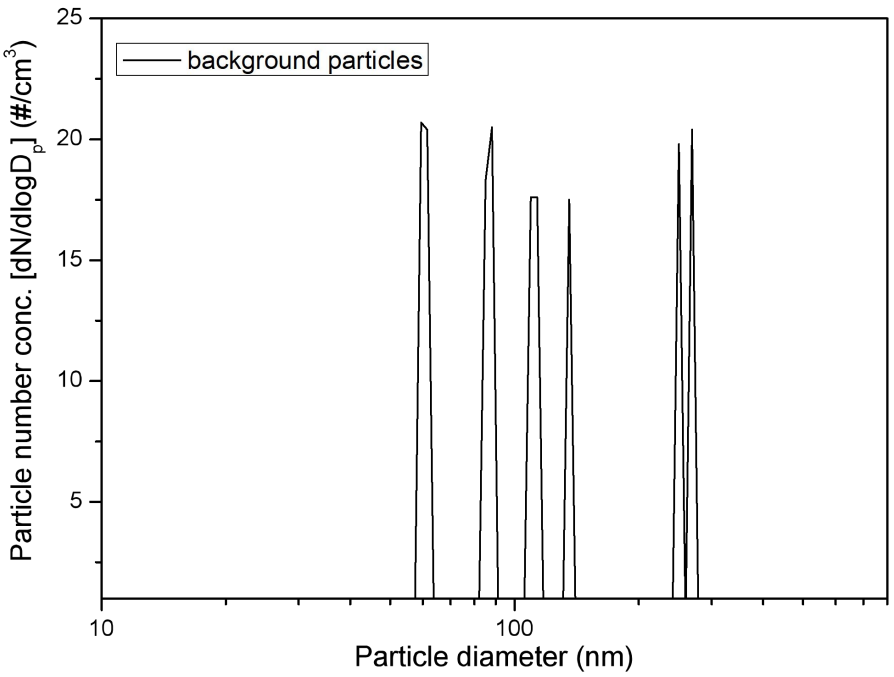

Fig. S2. Background particle number size distribution

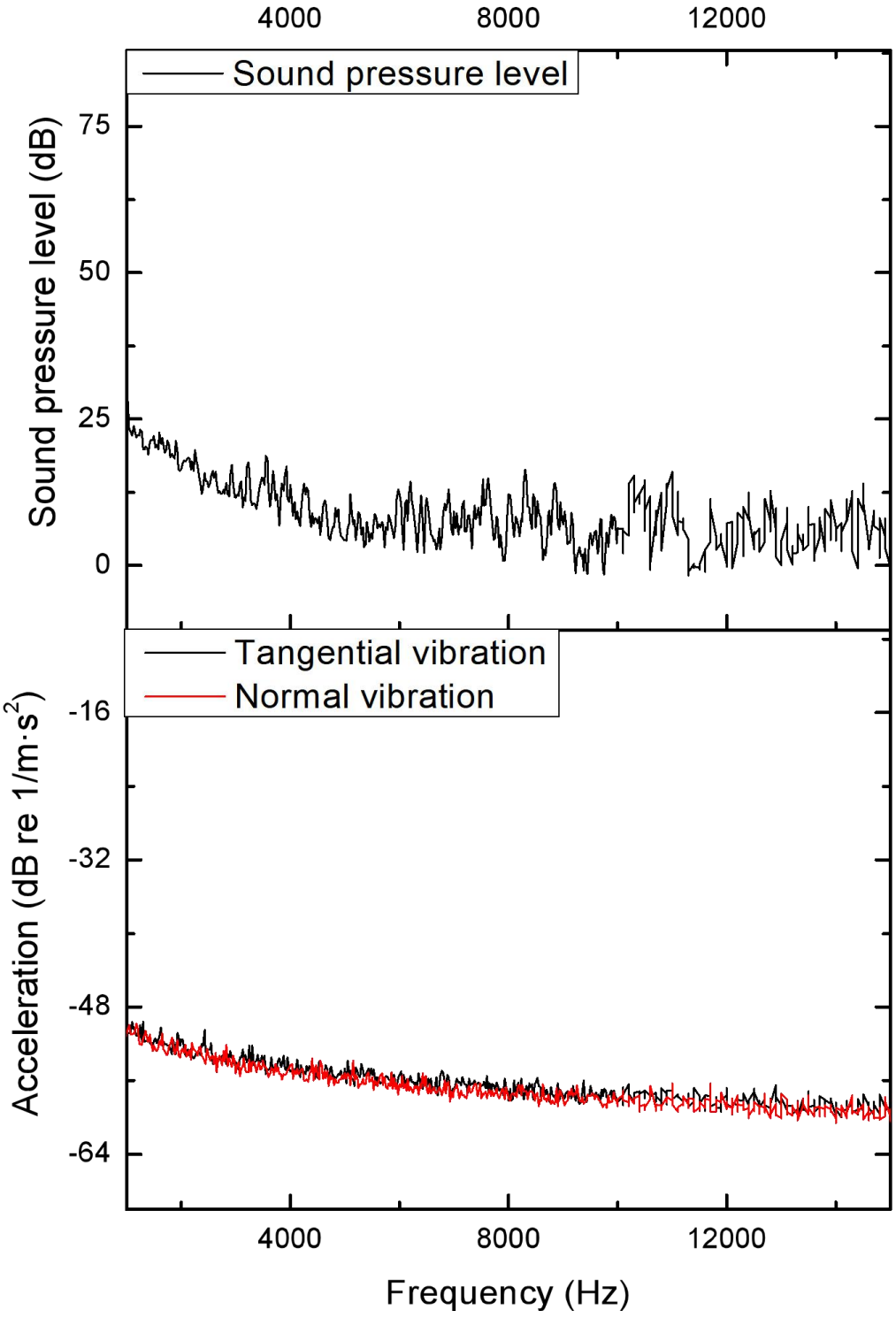

Fig. S3. SPL and acceleration spectra of background noise

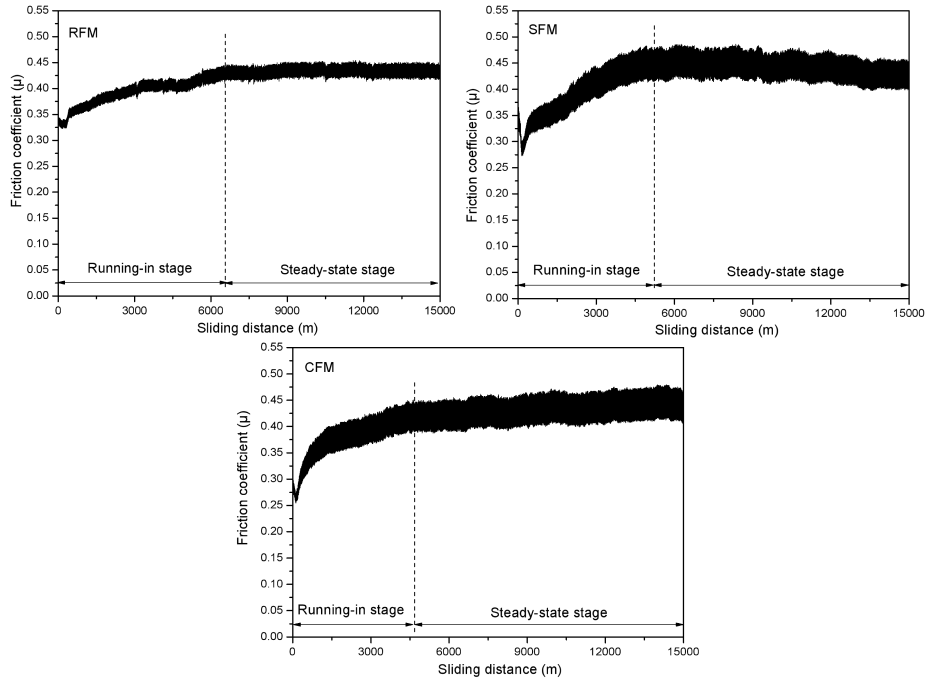

(a) 0.81 MPa

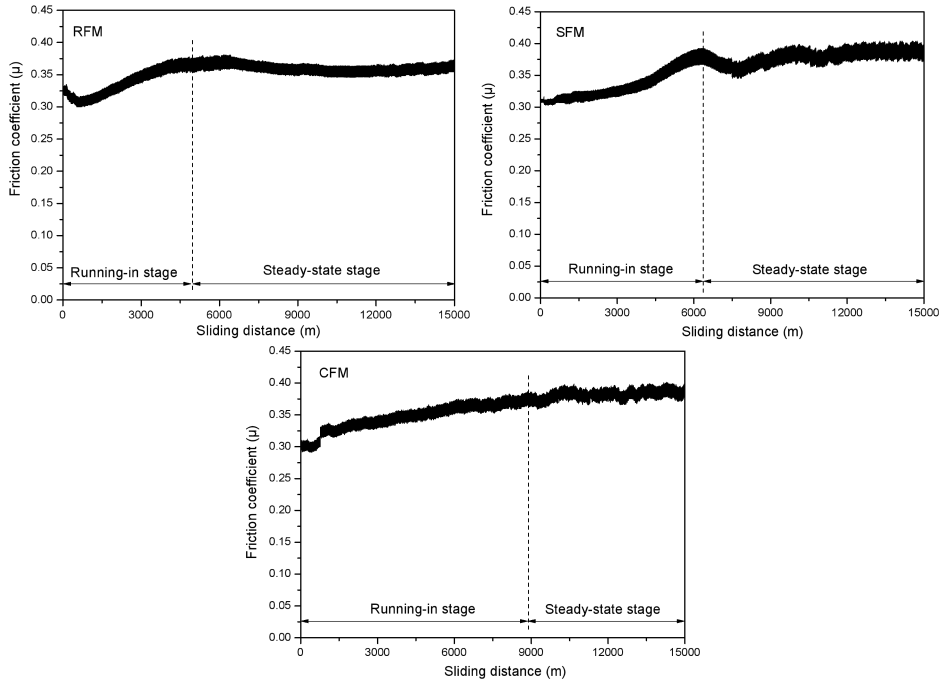

(b) 1.22 MPa

Fig. S4. Variations of friction coefficient during tests (Test modes 2 and 3)

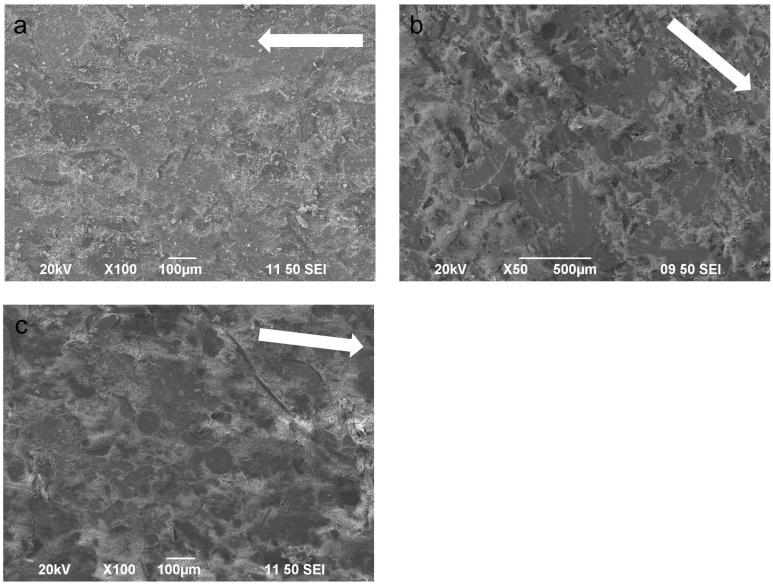

(a) 0.81 MPa

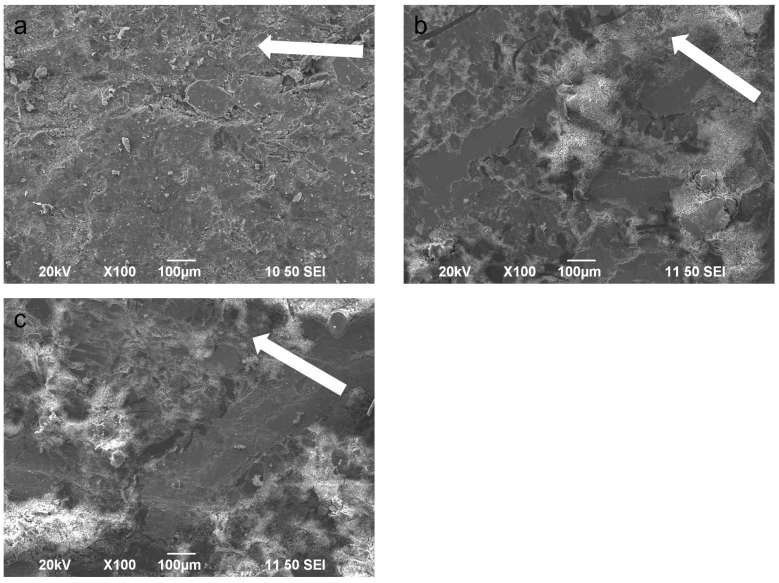

(b) 1.22 MPa

Fig. S5. SEM pictures of pin sample surfaces (a: RFM, b: SFM, c: CFM; white arrow indicating the sliding direction).

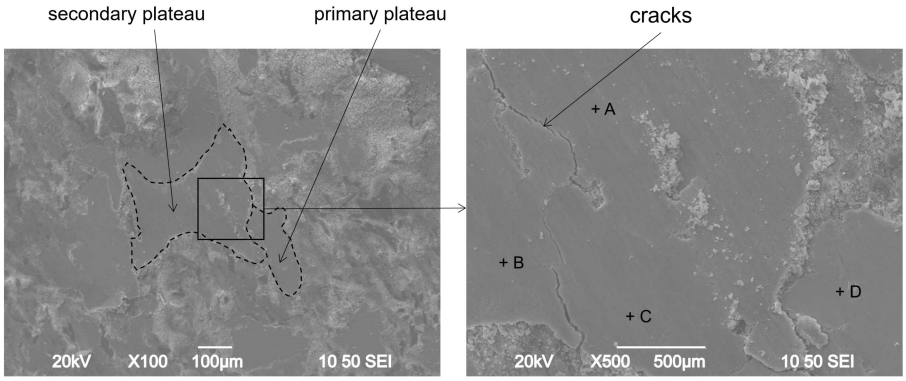

Spectrum A

Element	Weight%	Atomic%
O K	27.79	59.00
Si K	2.75	3.32
S K	1.98	2.10
Ca K	1.42	1.20
Fe K	49.95	30.38
Ba L	16.11	3.98
Totals	100.00	

Spectrum B

Element	Weight%	Atomic%
C K	15.45	34.00
O K	24.50	40.47
Si K	2.00	1.88
S K	1.28	1.06
Ca K	1.31	0.86
Fe K	39.38	18.64
Ba L	16.07	3.09
Totals	100.00	

Spectrum C

Element	Weight%	Atomic%
C K	13.07	31.07
O K	22.51	40.19
S K	1.48	1.31
Ca K	1.58	1.13
Fe K	44.64	22.83
Ba L	16.73	3.48
Totals	100.00	

Spectrum D

Element	Weight%	Atomic%
Fe K	97.79	99.09
Ba L	2.21	0.91
Totals	100.00	

Fig. S6. SEM pictures and EDXS point spectra of the SFM surface (Test mode 2)

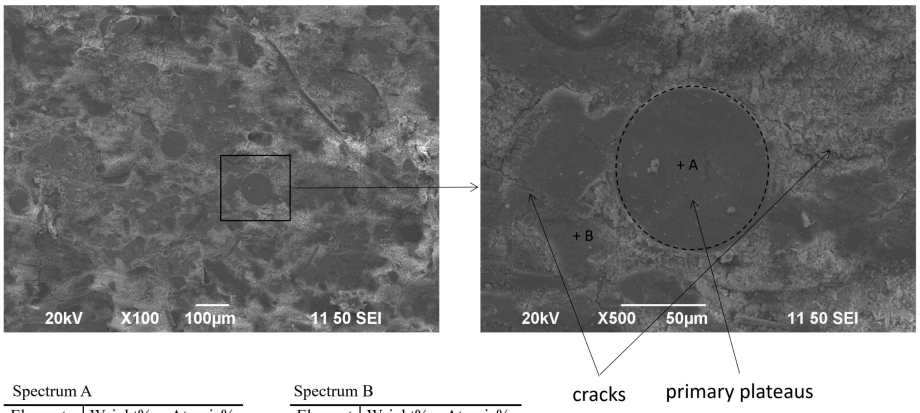

Spectrum A

Element	Weight%	Atomic%
C K	32.71	54.72
O K	22.56	28.33
Si K	6.69	4.79
S K	0.89	0.56
Ca K	6.93	3.47
Fe K	17.38	6.25
Ba L	12.85	1.88
Totals	100.00	

Spectrum B

Element	Weight%	Atomic%
C K	33.69	56.80
O K	23.04	29.16
Si K	2.96	2.13
S K	1.00	0.63
Ca K	3.08	1.55
Fe K	20.37	7.38
Ba L	15.86	2.34
Totals	100.00	

Fig. S7. SEM pictures and EDXS point spectra of the CFM surface (Test mode 2)

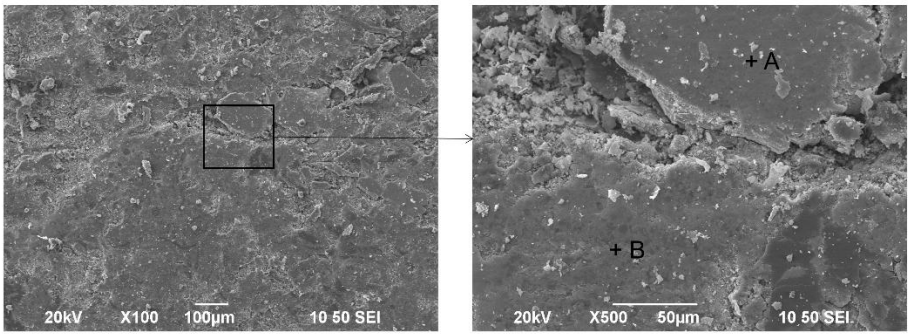

Spectrum A

Element	Weight%	Atomic%
C K	11.76	28.81
O K	19.70	36.21
Al K	1.38	1.50
Si K	7.35	7.70
Ca K	1.41	1.03
Fe K	8.81	4.64
Cu K	38.11	17.64
Ba L	11.49	2.46
Totals	100.00	

Spectrum B

Element	Weight%	Atomic%
C K	18.33	40.15
O K	21.63	35.57
Si K	7.61	7.13
S K	4.19	3.44
Ca K	3.07	2.01
Fe K	6.02	2.84
Cu K	6.11	2.53
Ba L	33.04	6.33
Totals	100.00	

Fig. S8. SEM pictures and EDXS point spectra of the RFM surface (Test mode 3)

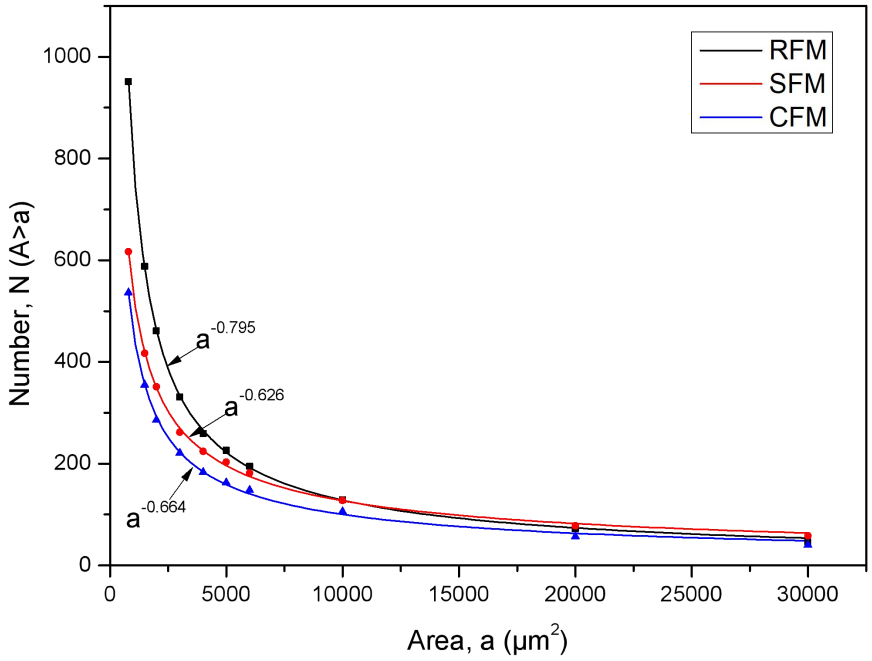

(a) 0.52 MPa

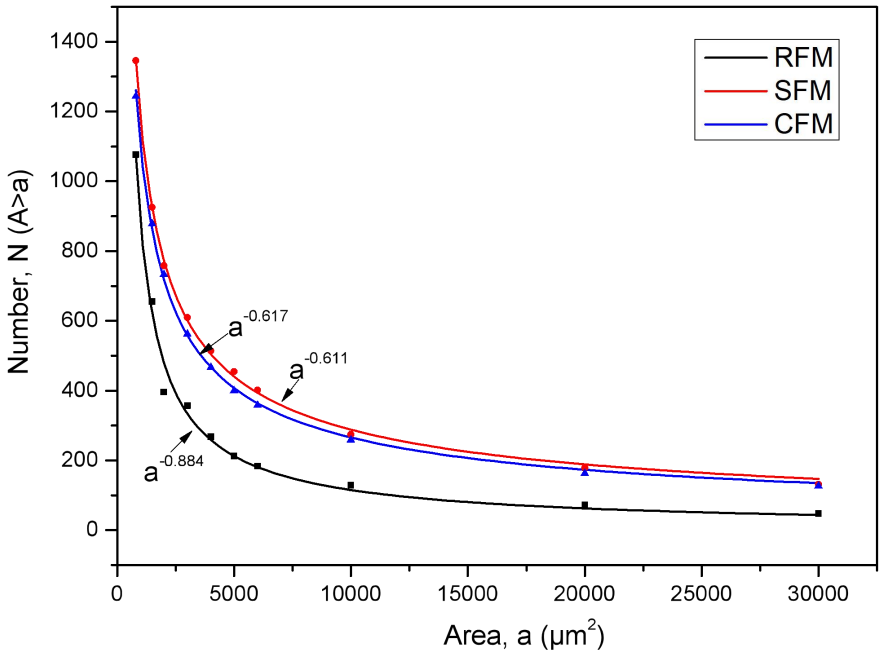

(b) 0.81 MPa

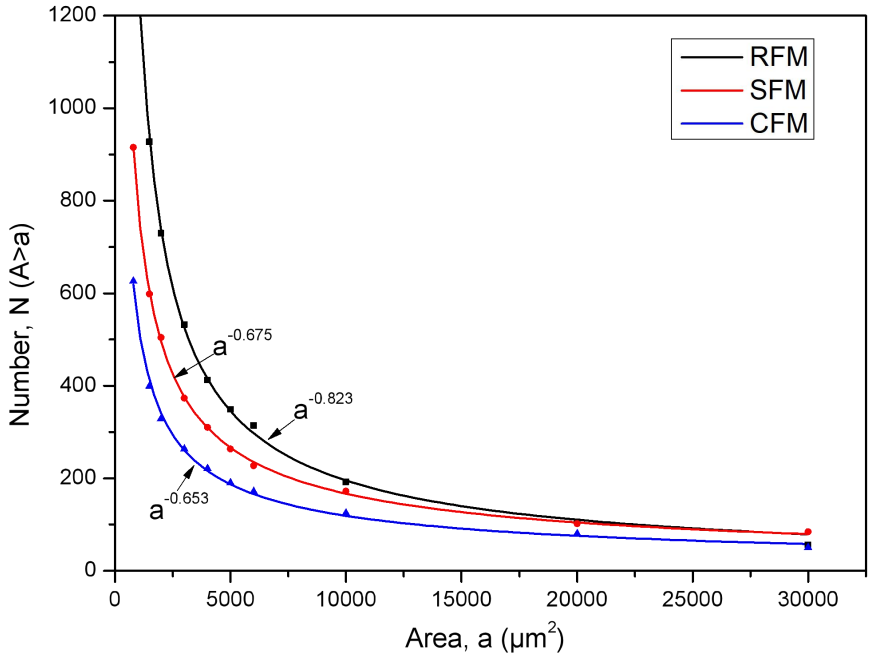

(c) 1.22 MPa

Fig. S9. Number-area distributions of friction layers on the pin surface

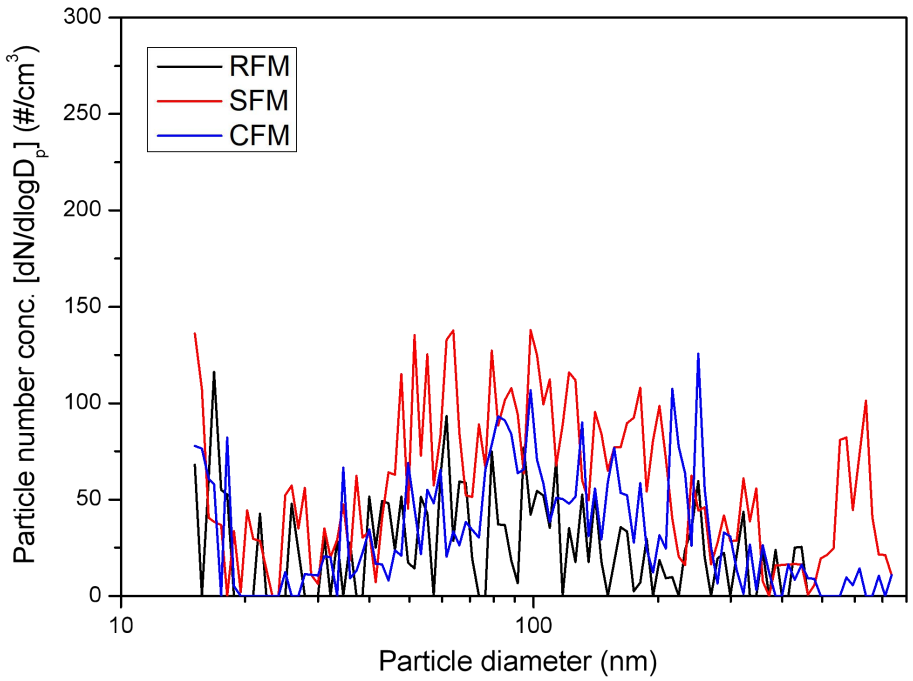

(a) 0.52 MPa

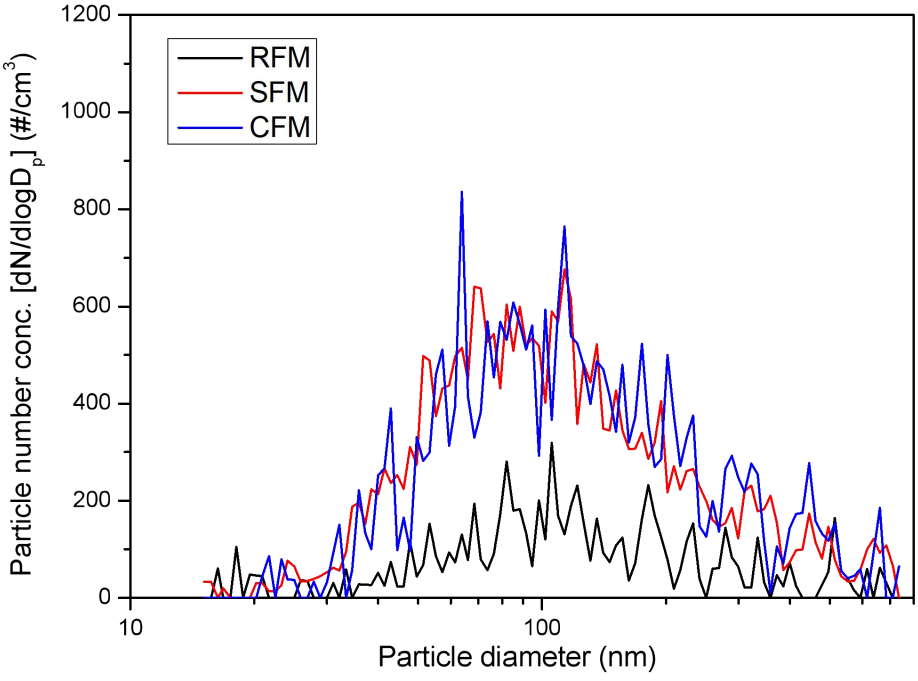

(b) 1.22 MPa

Fig. S10. Particle number size distributions at mode 1 and 3 tests

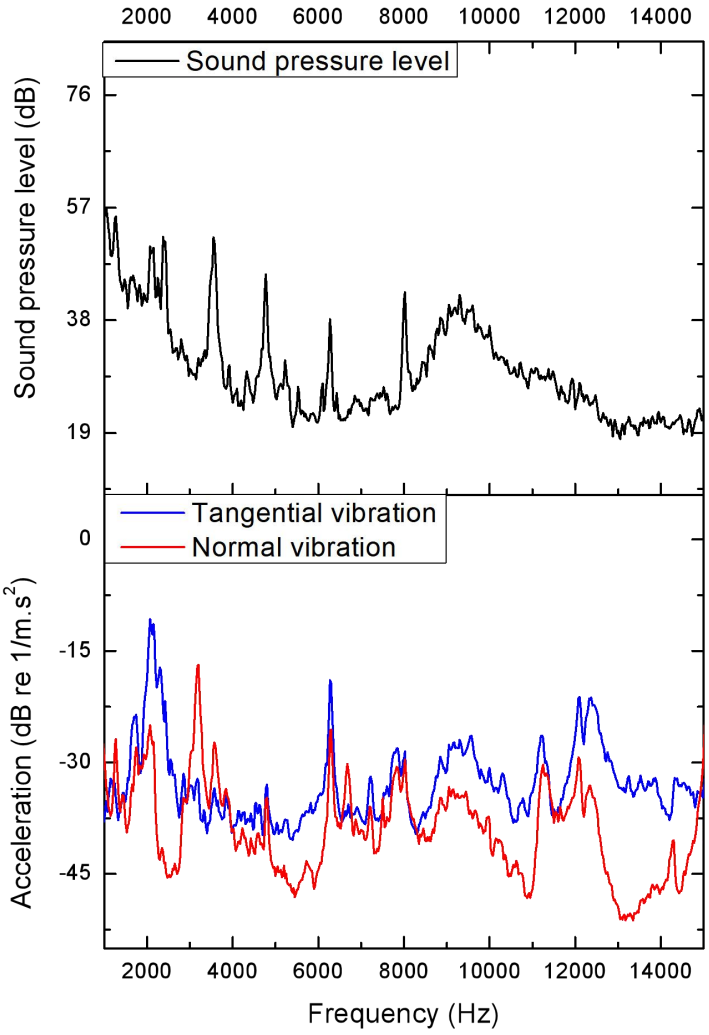
Sound pressure level
Sound pressure level (dB)
76
57
38
19
Tangential vibration
Normal vibration
Acceleration (dB re 1/m.s^2)
0
-15
-30
-45
2000
4000
6000
8000
10000
12000
14000
Frequency (Hz)

(a) 0.52 MPa

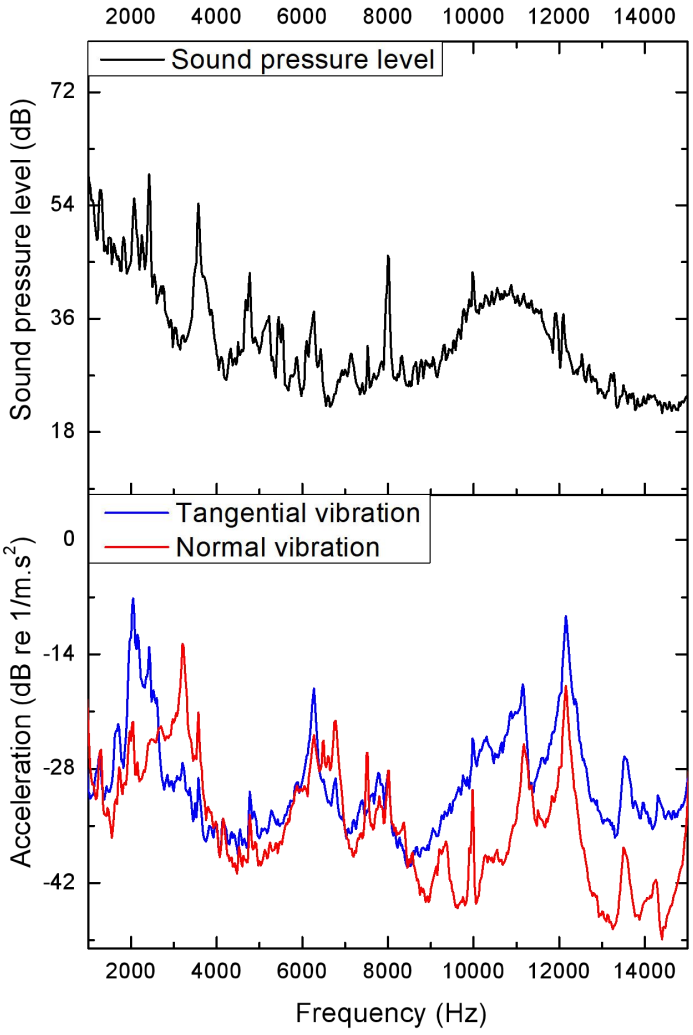
Sound pressure level
Sound pressure level (dB)
72
54
36
18
Tangential vibration
Normal vibration
Acceleration (dB re 1/m.s^2)
0
-14
-28
-42
2000
4000
6000
8000
10000
12000
14000
Frequency (Hz)

(b) 0.81 MPa

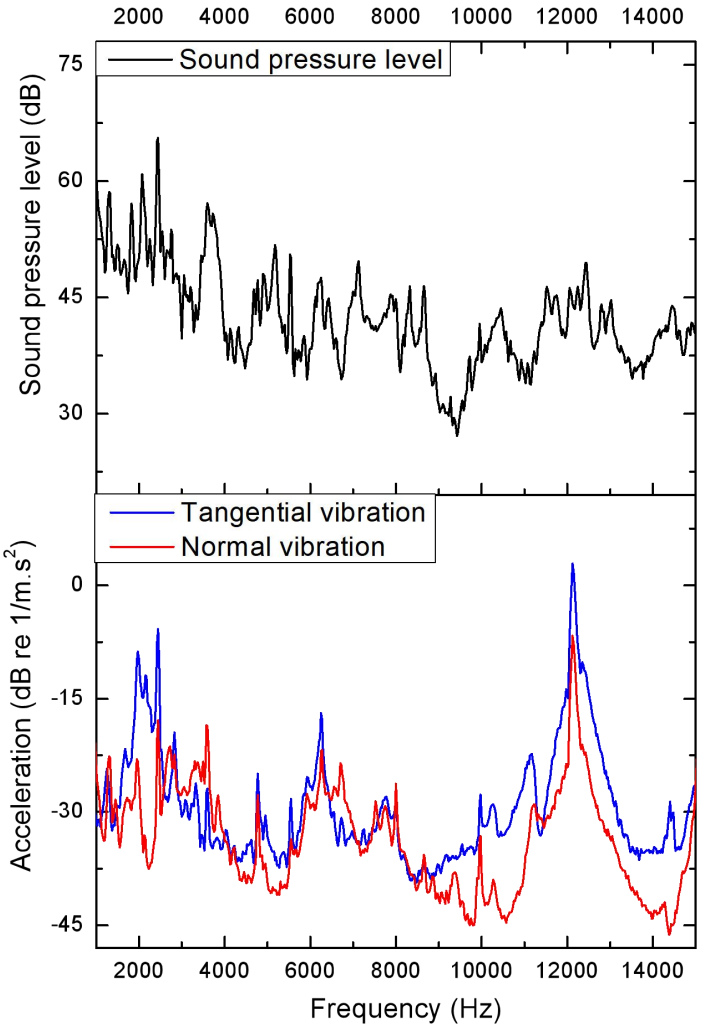

(c) 1.22 MPa

Fig. S11. SPL and acceleration spectra for RFM

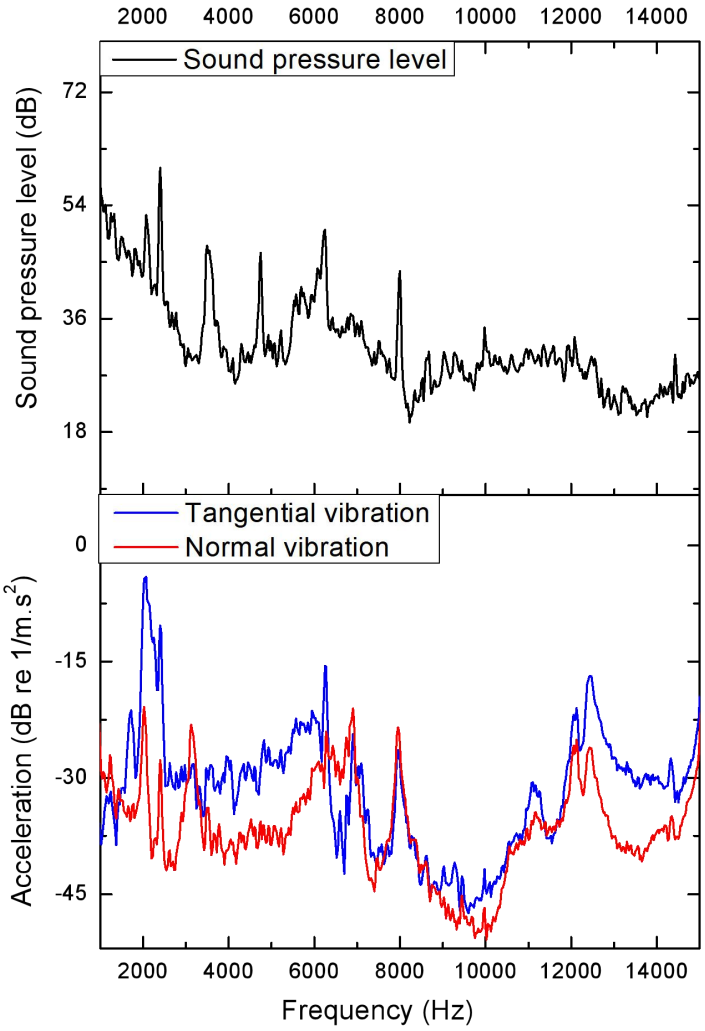
Sound pressure level
Sound pressure level (dB)
72
54
36
18
Tangential vibration
Normal vibration
Acceleration (dB re 1/m.s^2)
0
-15
-30
-45
2000
4000
6000
8000
10000
12000
14000
Frequency (Hz)

(a) 0.52 MPa

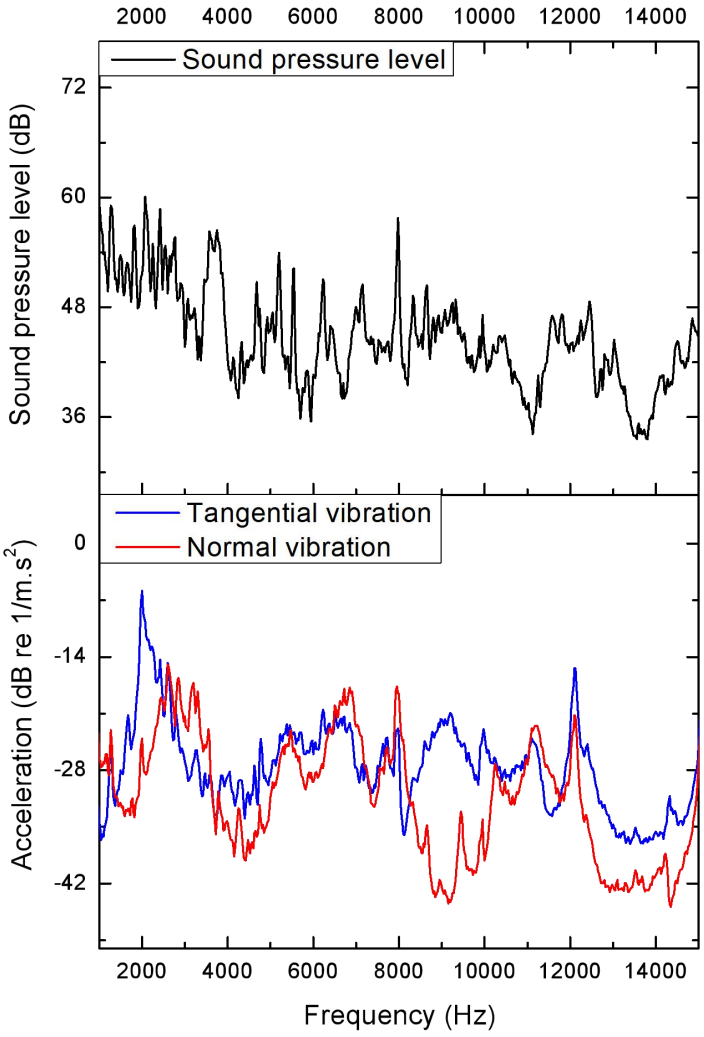

(b) 1.22 MPa

Fig. S12. SPL and acceleration spectra for SFM

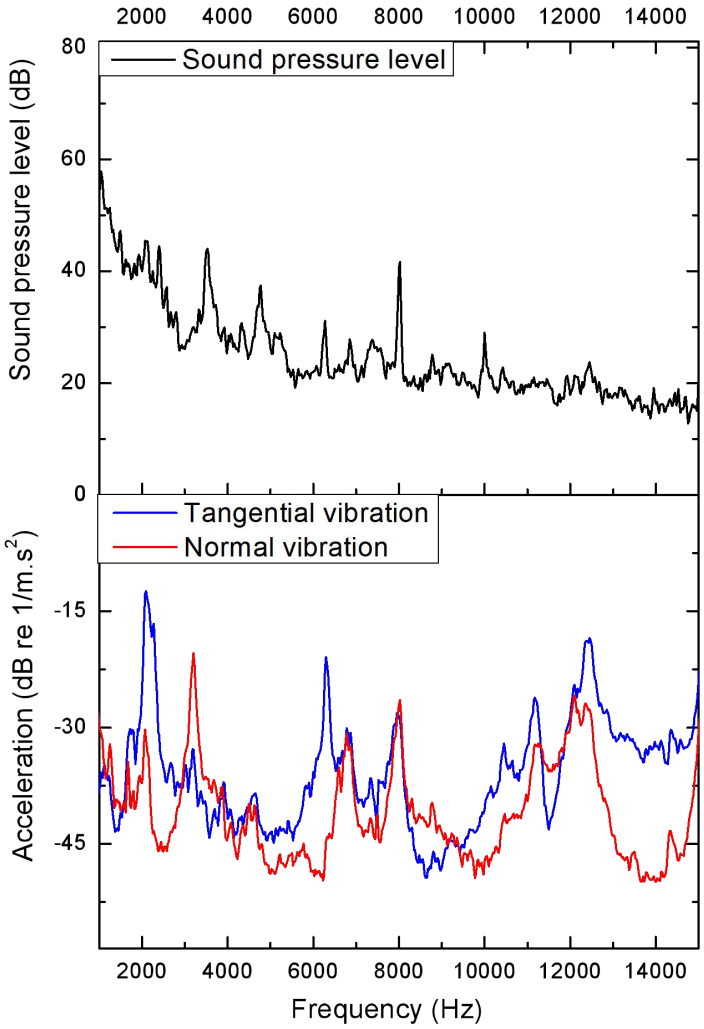
Sound pressure level
Sound pressure level (dB)
Tangential vibration
Normal vibration
Acceleration (dB re 1/m.s^2)
Frequency (Hz)
2000
4000
6000
8000
10000
12000
14000
80
60
40
20
0
-15
-30
-45

(a) 0.52 MPa

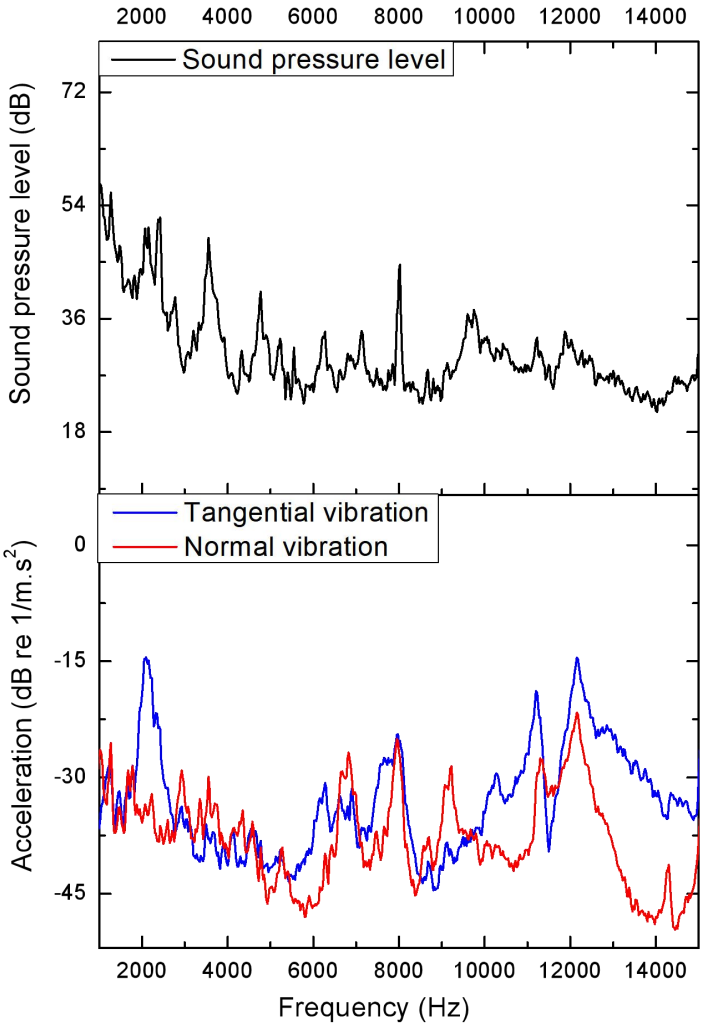
Sound pressure level
Sound pressure level (dB)
72
54
36
18
Tangential vibration
Normal vibration
Acceleration (dB re 1/m.s^2)
0
-15
-30
-45
2000
4000
6000
8000
10000
12000
14000
Frequency (Hz)

(b) 0.81 MPa

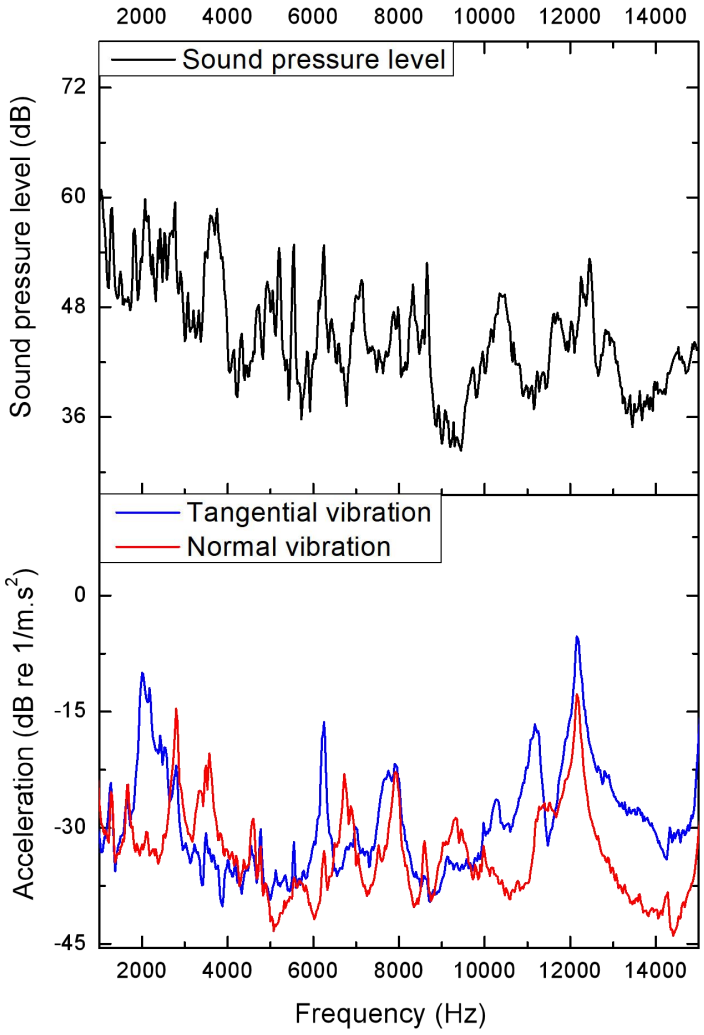

(c) 1.22 MPa

Fig. S13. SPL and acceleration spectra for CFM